Chapter 3

Two-Dimensional Velocity Analysis without Picking

3.1 INTRODUCTION AND OVERVIEW OF CHAPTER

Although the velocity analysis algorithm of the last chapter successfully determined interval velocities for single CMP gathers, it had one significant limitation: it did not allow for laterally varying velocities. Indeed, its application to laterally varying media leads to clearly incorrect interval velocities. Laterally variable media can be properly treated, however, by a more general version of the algorithm of the last chapter.

This more general version retains the overall structure of the simpler, laterally invariant algorithm, but two basic details are changed. First, the connection between interval slowness and stacking slowness can no longer rely on the assumption that stacking velocity equals rms velocity: this assumption is simply not valid for laterally variable velocities. Instead, the theory proposed here connects interval and stacking slownesses through the intermediary of traveltimes. This alternative theory produces the second basic change in the algorithm: CMP gathers cannot be considered independently. Instead, the stacking slownesses at all midpoints are considered simultaneously. The resulting algorithm is applied to a field-data example that shows strong lateral variation.

3.2 ILLUSTRATION OF PROBLEM

The basic, one-dimensional algorithm proposed in the last chapter encounters serious difficulties if the velocities show significant lateral variation. These difficulties are vividly illustrated with a field-data example. Figure 3.1 shows a stacked section from the Central Valley of California. A time sag is visible in the center of the section. This sag is known to be due to gas seeping upward from depth, and thus clearly corresponds to a low-velocity anomaly. Figure 3.2 shows the semblance panels for two different midpoints, one some distance to the left of the anomaly, the other at the same midpoint as

the anomaly. Overlaid on Figure 3.2 are the final stacking slowness curves derived by the iterative process of the last chapter.

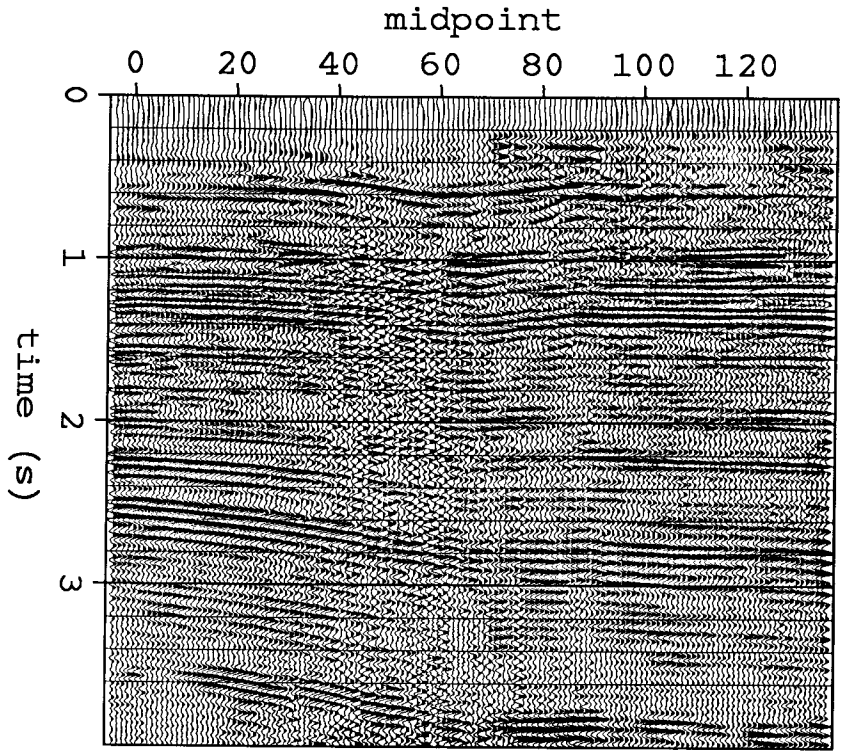

FIG. 3.1. Stacked section from the Central Valley of California. A time sag is visible in the center of the section; this sag is clearly due to a low-velocity anomaly.

The results seems perfectly reasonable until one looks at the interval slowness models. Figure 3.3a shows the model for the midpoint away from the anomaly, Figure 3.3b for the midpoint at the anomaly. The derived interval slownesses are actually smaller for the midpoint of the anomaly, than those for the midpoint away from the anomaly. This last statement, when expressed in terms of velocity instead of slowness, says that the time sag corresponds to a high velocity zone; something is clearly wrong with these models.

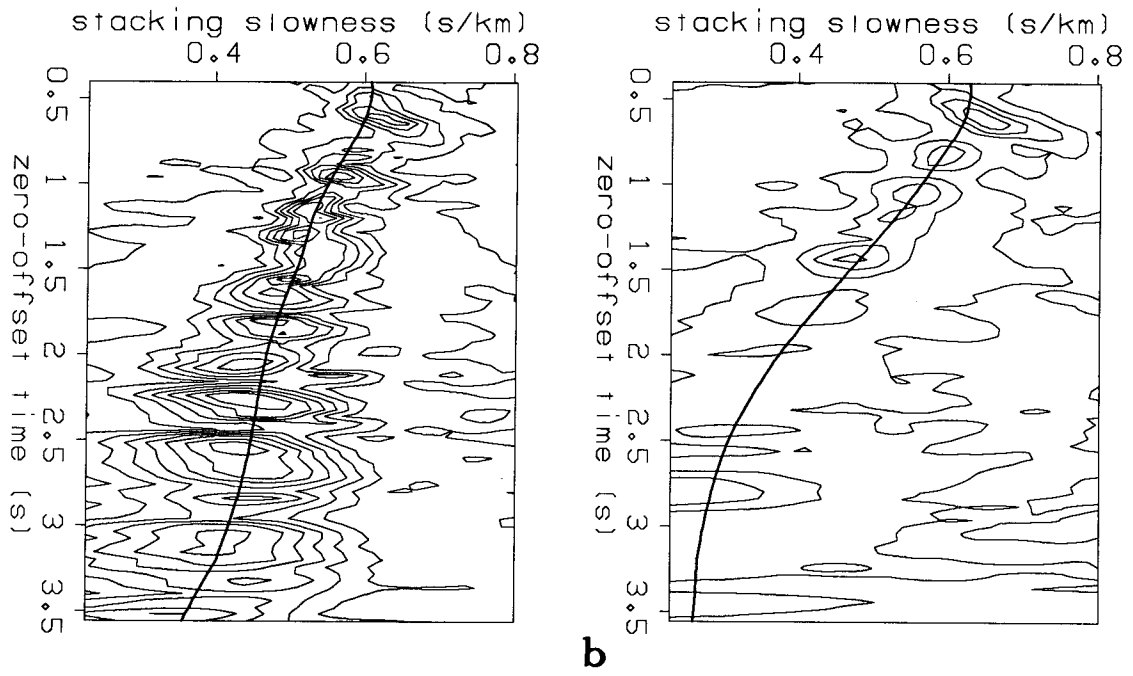

FIG. 3.2. Semblance panels for two different midpoints. a) Midpoint 10, away from anomaly. b) Midpoint 60, at anomaly. Overlaid on each are the final stacking slowness curves derived by the iterative process of the last chapter.

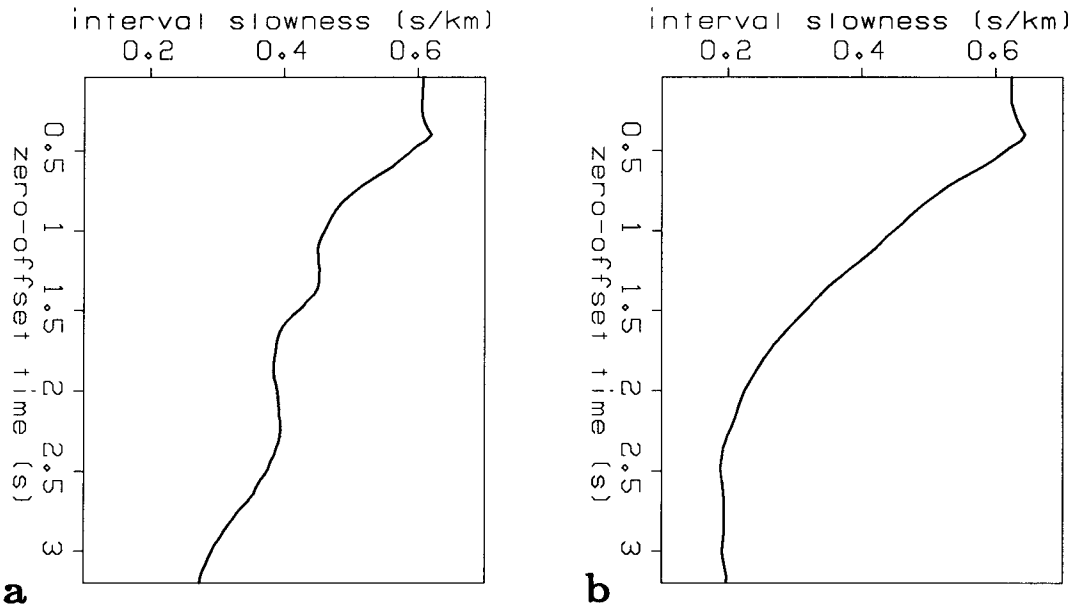

FIG. 3.3. Results of the one-dimensional algorithm. a) Interval slowness model for midpoint 10. b) Interval slowness model for midpoint 60. The one-dimensional algorithm gives lower interval slownesses (higher velocities) at the anomaly (midpoint 60).

3.3 TWO-DIMENSIONAL FORMULATION: THEORY

The problem with the method of the last chapter arises because an underlying assumption—that stacking velocities are equal to rms velocities—is not valid for laterally varying media. This assumption was fundamental to the derivation of the relationship between interval slownesses and stacking slowness, that is, $\mathbf{w}(\mathbf{m})$ of equation (2.1). This relationship must be re-derived if the algorithm is to be applied to laterally varying media.

The basis of the more general $\mathbf{w}(\mathbf{m})$ is an interpretation of stacking velocity as something other than rms velocity. Stacking velocity, or rather stacking slowness, is just a parameter describing a hyperbolic summation trajectory. The value of this parameter that corresponds to the largest semblance will be determined by the traveltimes. Thus, traveltimes serve as an intermediary between interval and stacking slownesses; $\mathbf{w}(\mathbf{m})$ should more properly be written as $\mathbf{w}[\mathbf{t}(\mathbf{m})]$.

One could calculate these stacking slownesses $\mathbf{w}$, due to the model $\mathbf{m}$, by first ray-tracing through $\mathbf{m}$ for the traveltimes $\mathbf{t}$, then fitting hyperbolas to these $\mathbf{t}(\mathbf{m})$, to determine the $\mathbf{w}[\mathbf{t}(\mathbf{m})]$. For certain models, this calculation can be greatly simplified by use of a linear approximation to $\mathbf{w}[\mathbf{t}(\mathbf{m})]$. This linear approximation was first proposed by Lynn (1980), then more fully developed by Loinger (1983). Then, in Rocca and Toldi (1983), we showed how this linear theory could be used in an inversion procedure.

The linear theory calculates the change in stacking slowness that is due to a change in the interval-slowness model from a reference model. Figure 3.4 shows a few of the raypaths of one CMP gather, for the simple reference model of a single, flat reflector and constant interval slowness. A change in the interval slowness in the small box at $(y_a\,,\,z_a)$, will affect the traveltime of the ray that goes through the box. This ray will be at some offset x. Because of this change in traveltime at offset x, the value of the stacking-slowness parameter describing the best-fit hyperbola will also change.

The total change in the stacking slowness at midpoint y, for the reflector at depth z, is the integral over the "fan" shown in Figure 3.4.

$$\Delta w(y\,,\,z) \;=\; \int_{y_a}\int_{z_a} G(y\,,\,z\,,\,y_a\,,\,z_a)\,\Delta w_{in}(y_a\,,\,z_a)\,dz_a\,dy_a \quad . \tag{3.1}$$

$\Delta w_{in}(y_a\,,\,z_a)$ is the perturbation in interval slowness at the point $(y_a\,,\,z_a)$. Each such perturbation is weighted according to the impulse response $G(y\,,\,z\,,\,y_a\,,\,z_a)$. This impulse response, which is derived in Chapter 4, is

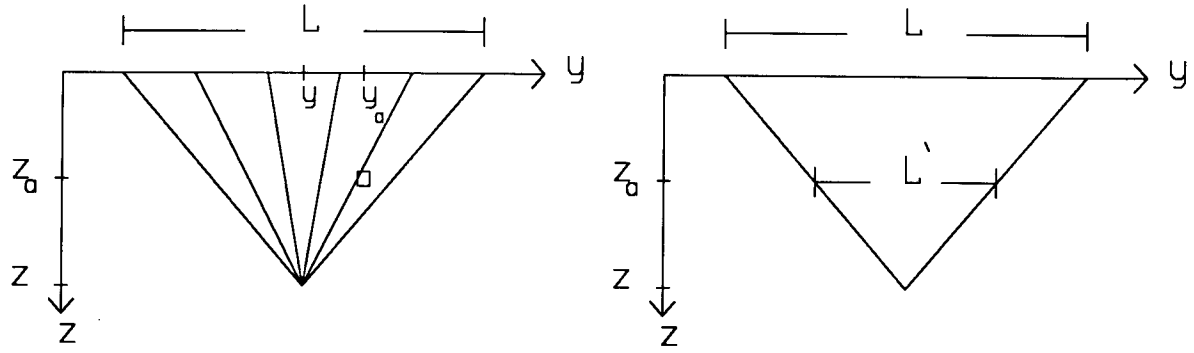

FIG. 3.4. Geometry for a constant background slowness and a flat reflector. Shown are a few raypaths for the CMP gather at y. The maximum offset is L; L' is the projection along the far offset ray of L to depth z_a. The impulse of anomalous interval slowness has coordinates y_a, z_a.

$$G(y, z, y_a, z_a) = \frac{15z}{L^2 L'} \left[3\left(\frac{2(y_a - y)}{L'} \right)^2 - 1 \right] \left[1 + \frac{L^2}{4z^2} \left(\frac{2(y_a - y)}{L'} \right)^2 \right] . \qquad (3.2)$$

$$\text{for } \left| y_a - y \right| < \frac{L'}{2}$$

$$= 0 \qquad \text{for } \left| y_a - y \right| > \frac{L'}{2}$$

L' is the width of the "fan" at depth z_a, and thus acts as the aperture of the filter G.

Equation (3.2) was derived for a constant background velocity. For a depth-variable background velocity, the impulse response G looks exactly like equation (3.2). The only variation is in the definition of L' : instead of following the straight-line raypath of Figure 3.4, L' follows the bent raypath corresponding to the depth-variable velocity. The linear theory can also be extended to allow for a laterally variable background or for dipping reflectors. These extensions are discussed in Chapter 4. For the examples here, however, the background model is assumed to be composed of flat reflectors, and have a laterally invariant velocity distribution.

A discrete form of equation (3.1) is derived, if the model is described in terms of a set of basis functions $h_k(y_a, z_a)$. That is, the interval slowness w_{in} at (y_a, z_a) can be

written as

$$w_{in}(y_a, z_a) = \sum_k m_k h_k(y_a, z_a) . \tag{3.3}$$

The m_k are the expansion coefficients. The background model $\hat{w}_{in}(y_a, z_a)$ can likewise be expanded in terms of the parameters $\hat{\mathbf{m}}$. Substituting equation (3.3) into equation (3.1) gives the discrete form of the linear theory:

$$w_{ij}(\mathbf{m}) = w_{ij}(\hat{\mathbf{m}}) + \sum_k G_{ijk}(m_k - \hat{m}_k) . \tag{3.4}$$

The subscript i refers to the reflector at depth z_i, j refers to the midpoint y_j. The matrix element G_{ijk} is

$$G_{ijk} = \int_{y_a} \int_{z_a} G(y_j, z_i, y_a, z_a) h_k(y_a, z_a) dz_a \, dy_a . \tag{3.5}$$

The basis functions $h_k(y_a, z_a)$ can be chosen to suit the background model. For the flat reflectors and laterally invariant background considered here, G depends only on $(y_a - y_j)$: the integral over midpoint in equation (3.5) is a convolution. With the basis functions chosen to be sinusoids laterally, this convolution becomes a multiplication of the basis function by the Fourier transform of G. This choice of basis functions thus allows the insight gained in the study of the Fourier transform of G in Chapter 4 to be directly applied to the velocity analysis algorithm. Because of the flat reflectors, the basis functions are chosen to be thin strips in depth.

3.4 TWO-DIMENSIONAL FORMULATION: INTERACTION WITH DATA

In order to allow for lateral variation in the interval-slowness model $\mathbf{m}$, the previous section derived a general form of the expression $\mathbf{w}(\mathbf{m})$. Otherwise, the structures of the laterally-variant and laterally-invariant algorithms are the same. In particular, the objective function is fundamentally unchanged: evaluate the model $\mathbf{m}$ by looking at the power in the stack formed according to $\mathbf{w}(\mathbf{m})$. That is, the $\mathbf{w}(\mathbf{m})$ define a set of hyperbolic curves over offset and time. These curves can be used as summation trajectories; the larger the power in the resulting sum, the better the model $\mathbf{m}$.

If semblance is used in place of stack power, the objective function can then be written as:

$$Q(\mathbf{m}) = \sum_j \sum_i S(w_{ij}(\mathbf{m}), \tau_i, y_j) . \tag{3.6}$$

This objective function is much like the simpler, one-dimensional version (equation

(2.4)); the only change is the additional sum over midpoint (i.e. over j). For each j, the inner sum is a sum along the curve $w_{ij}(\mathbf{m})$, through the semblance panel $S(w_{ij}(\mathbf{m}), \tau_i, y_j)$. This sum is then added to the analogous results from all other midpoints.

If the semblance panels from all midpoints are lined up one behind the other, they form a cube of semblance values, $S(w, \tau, y)$ (Figure 3.5). As i and j range over their full set of values, the $w_{ij}(\mathbf{m})$ describe a surface inside the cube: to evaluate the model $\mathbf{m}$, equation (3.6) sums the semblance values lying on this surface.

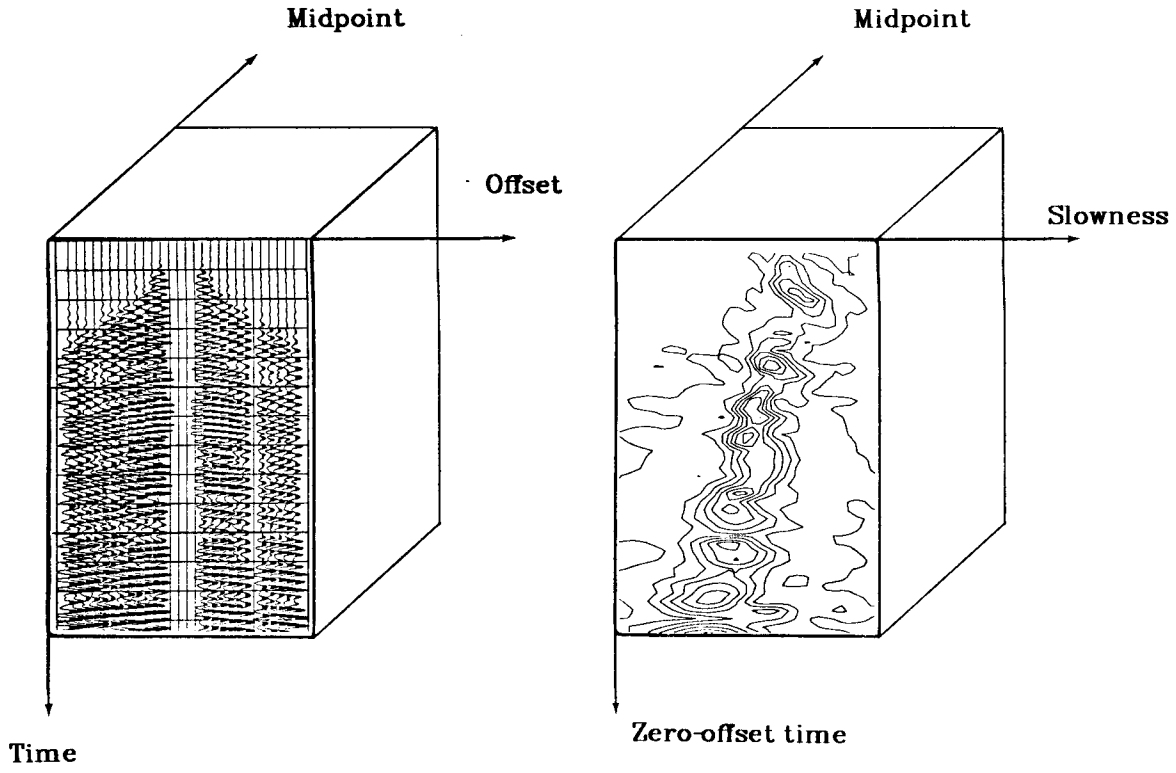

FIG. 3.5. The data $D(x, t, y)$ are transformed to a cube of semblance values $S(w, \tau, y)$. The contours of semblance for the front face of the cube are shown; this is a standard semblance panel for one midpoint.

If the data contain flat reflectors, a simpler interpretation of equation (3.6) is possible. The semblance values corresponding to flat reflectors will lie roughly in a set of horizontal planes of the semblance cube. Thus, for one such reflector, the semblance values can be extracted by a horizontal slice through the cube at the appropriate zero-offset time. Figure 3.6 shows one horizontal slice, and the contours of semblance for the extracted plane. Figure 3.6 is a so-called horizon, or event velocity-analysis.

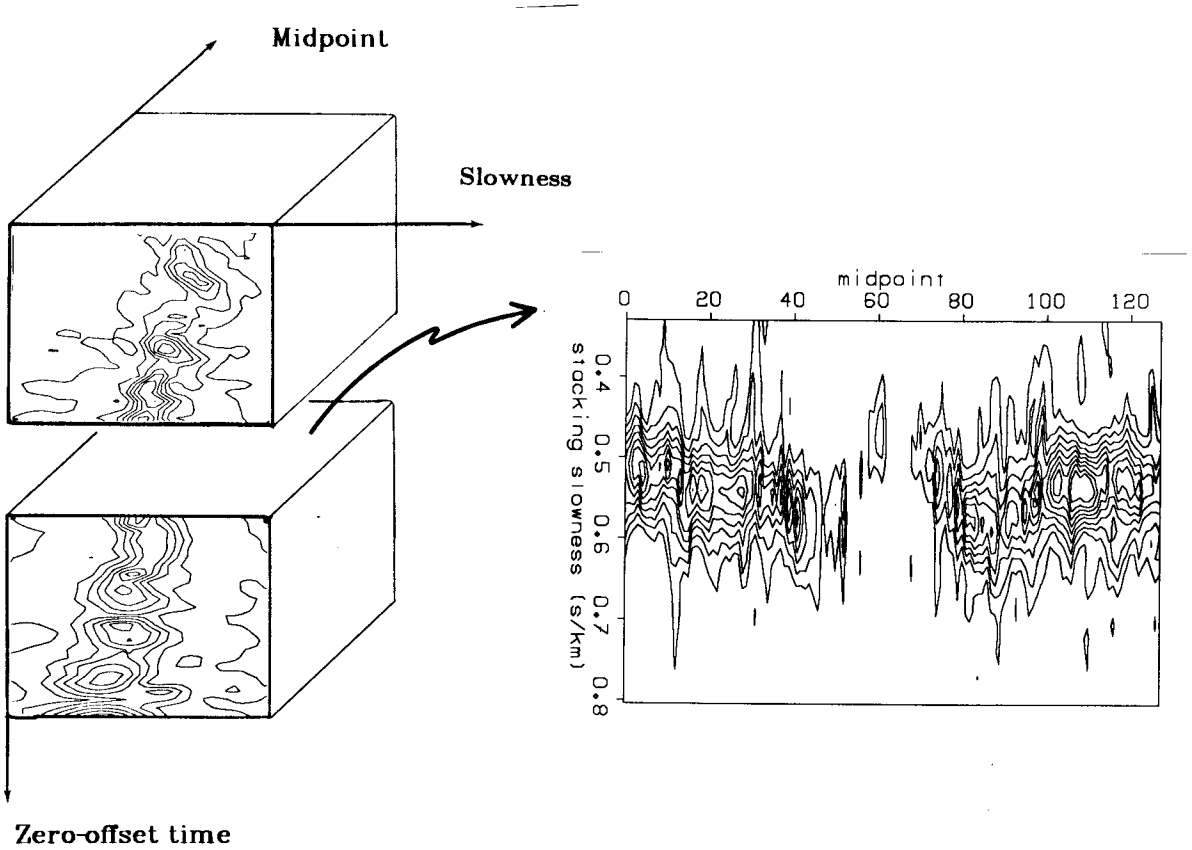

FIG. 3.6. The semblance values for a flat reflector can be extracted by a horizontal slice through the semblance cube. The extracted plane of semblance as function of stacking slowness and midpoint is shown on the right.

This event-velocity analysis enters directly into the evaluation of a model, if the order of summation in equation (3.6) is reversed. That is,

$$Q(\mathbf{m}) = \sum_i \sum_j S(w_{ij}(\mathbf{m}), \tau_i, y_j) . \qquad (3.7a)$$

Now as the inner sum, formed for a fixed value of i and thus τ_i, ranges over the index j, the semblance values lying along the curve $w_{ij}(\mathbf{m})$ are summed. That is, fixing i fixes the time plane; the $w_{ij}(\mathbf{m})$ values then define a summation curve in this plane. Figure 3.7 shows one such curve, plotted over the event velocity-analysis of Figure 3.6. The full velocity-analysis algorithm will try to drive this curve to the peaks of Figure 3.7. The outer sum, over i, then totals the values for all events considered.

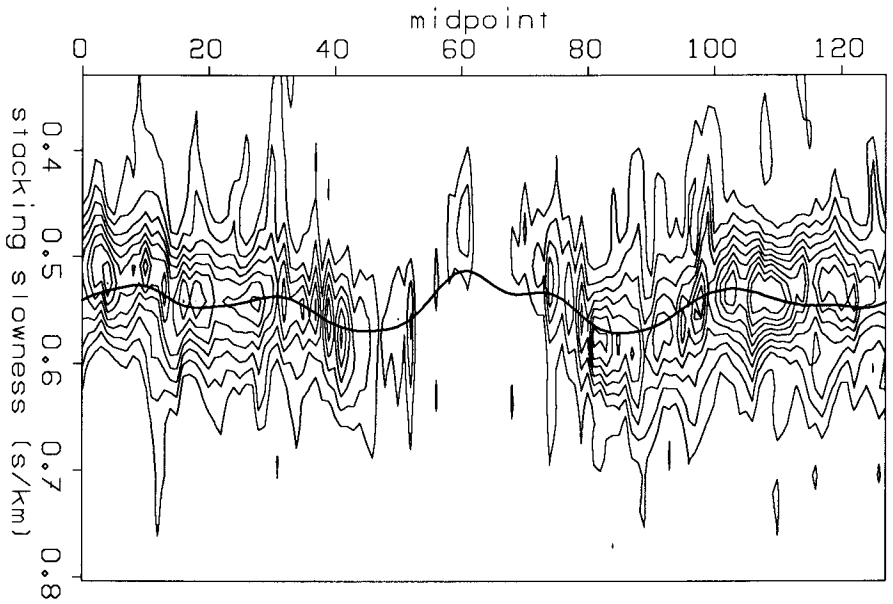

FIG. 3.7. For fixed i, $w_{ij}(\mathbf{m})$ defines a summation curve through the i^{th} event velocity analysis. The closer this curve comes to the peaks, the better the model $\mathbf{m}$.

Only for flat reflectors and laterally invariant velocities can an event velocity-analysis be extracted as a single horizontal slice through the semblance cube. For dipping reflectors, the event velocity-analysis can likewise be extracted as a slice from the semblance plane. This slice will not be horizontal, but rather must approximately follow the zero-offset times of the event. For application to strongly dipping events, equation (3.7a) can thus be rewritten explicitly as a sum over the event velocity-analyses:

$$Q(\mathbf{m}) = \sum_i \sum_j S(w_{ij}(\mathbf{m}), \tau_i(y_j), y_j) . \qquad (3.7b)$$

$\tau_i(y_j)$ is the zero-offset time of the i^{th} event at the j^{th} midpoint; τ_i is dependent on y because of the dip. Then, the outer sum over i in equation (3.7a) just adds up the results from the different dipping events.

For data with flat reflectors, but laterally varying velocities, equation (3.7a) can be used directly as written. When there is significant lateral variation of velocity, the location of the semblance values corresponding to a flat reflector will vary in time. Nonetheless, this time variation can be ignored, if the semblance values are sufficiently smoothed over time. Then, the time of the horizontal plane need only roughly match that of the event. Thus, when there are laterally variable velocities, the use of a long smoother in the semblance calculation, followed by a correspondingly coarse sampling in time, is appropriate.

Suppose that each horizontal slice of this coarsely-sampled semblance cube is assumed to contain an event. If several reflections have been smoothed together into the one time plane, then the algorithm will be working with an average event. Because of this averaging, there is clearly a trade-off between the sample rate in time and vertical resolution of the model. Those time planes that do not contain any reflectors will contribute little to the sum of equation (3.7a). Thus, when applied to data containing events that are roughly flat, yet have laterally variable velocities, equation (3.7a) leads to a fully automatic velocity-analysis algorithm.

The incorporation of laterally variable models into the velocity-analysis algorithm of the previous chapter thus requires two changes: first, the theory connecting interval slowness and stacking slowness, $\mathbf{w}(\mathbf{m})$, must be generalized to allow for the lateral variation. Second, this new theory requires that all midpoints be considered at once. Neither of these changes requires that the equations of the gradient-search algorithm be rewritten. All that is required is that the new $\mathbf{w}(\mathbf{m})$ be used, and that the stacking slowness now carry two indices, one for the zero-offset time and one for the midpoint. Thus, for example, the ij^{th} component of the gradient with respect to stacking slowness becomes

$$(\nabla_{\mathbf{w}} Q)_{ij} \;=\; \frac{S\left(w_{ij}(\mathbf{m}) + \Delta w\,,\, \tau_i\,,\, y_j\right) - S\left(w_{ij}(\mathbf{m}),\, \tau_i\,,\, y_j\right)}{\Delta w}\;. \tag{3.8}$$

Furthermore, the gradient with respect to the model is

$$\nabla_{\mathbf{m}} Q \;=\; \mathbf{G}^T\, \nabla_{\mathbf{w}} Q\;. \tag{3.9}$$

with $\mathbf{G}$ now specified by equation (3.5).

For the one-dimensional case, three enhancements to the basic steepest-ascent algorithm were proposed: smoothing over stacking slowness, using a conjugate-gradient instead of a simple gradient algorithm, and modifying the objective function to incorporate a priori information about the model. Of these three enhancements, only the incorporation of a-priori information is different for the two-dimensional algorithm.

Recall from equation (2.17a) that the a priori information was incorporated into the objective function through the addition of a model penalty-function. To force the ascent algorithm to try for a smooth model, this additional function made the algorithm pay a penalty proportional to the square of the derivative with depth of the model. That is, for the one-dimensional case,

$$Q'_{1\text{-}D}(\mathbf{m}) = \sum_i S(w_i(\mathbf{m}), \tau_i) - \beta\, \mathbf{m}^T \mathbf{D_z}^T \mathbf{D_z}\mathbf{m} . \tag{3.10}$$

Equation (3.10) has explicitly included the derivative matrices $\mathbf{D_z}$; note then, that in equation (2.17a) $\mathbf{D_z}^T \mathbf{D_z}$ produced the tridiagonal matrix $Tri(-1, 2, -1)$. The two-dimensional analog of equation (3.10) can be written as

$$Q'_{2\text{-}D}(\mathbf{m}) = \sum_i \sum_j S(w_{ij}(\mathbf{m}), \tau_i, y_j) - \beta \mathbf{m}^T \left(\mathbf{D_z}^T \mathbf{D_z} + \mathbf{D_y}^T \mathbf{D_y} \right) \mathbf{m} . \tag{3.11}$$

Now the model penalty-function is based on the magnitude of the gradient of the model; the model pays a penalty for not being smooth in both z and y. The parameter β specifies the weight given to this penalty function.

The model penalty-function incorporates the a priori information into the objective function. Thus, the matrix $\left(\mathbf{D_z}^T \mathbf{D_z} + \mathbf{D_y}^T \mathbf{D_y} \right)$ is an approximation to the inverse of the a priori model-covariance matrix; this particular approximation describes the expected smoothness of the model in a simple way. This smoothness term determines those parts of the model which influence the data weakly.

Note that this particular choice of penalty term is itself insensitive to certain components of the model. Multiplying the model by the matrix $\left(\mathbf{D_z}^T \mathbf{D_z} + \mathbf{D_y}^T \mathbf{D_y} \right)$ takes the Laplacian of the model. Thus, components of the model which are solutions to Laplace's equation can occur and not be affected by this penalty term. These components are of the form $\exp(iky)\exp(kz)$.

3.5 FIELD DATA EXAMPLE: DETERMINATION OF MODEL

This two-dimensional algorithm can be applied to the dataset with the time sag, which earlier served to illustrate the problems encountered by the one-dimensional algorithm. Figure 3.8 shows the shallow part of the stacked section; once again the time sag is clearly visible. The cause of the anomaly is known to be gas seeping upward from depth, but little is known about the detailed depth distribution.

The goal of the velocity-analysis algorithm is to determine the amplitude and depth distribution of the low-velocity anomaly. Because the reflectors are flat, the event

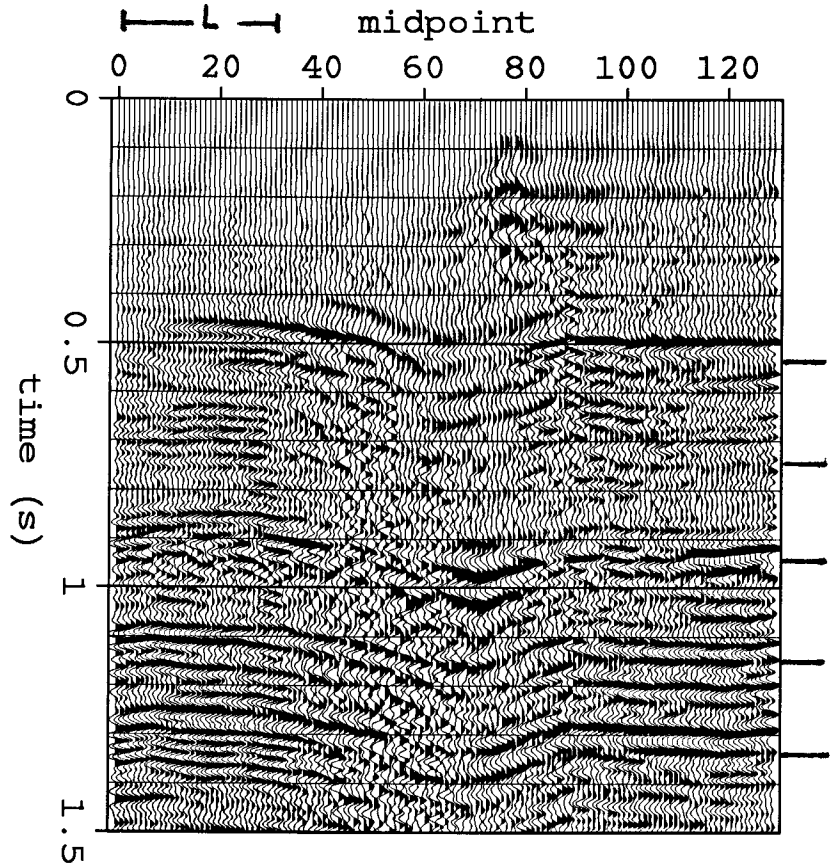

FIG. 3.8. Shallow part of stacked section from Central Valley of California. The tick marks on the right side show the reflectors that were used in this example. The cable length is marked on the top of the section.

velocity-analyses are extracted as horizontal slices through the semblance cube. These slices are taken at regular time intervals, with a spacing corresponding to the length of the time smoothing in the semblance calculation; for this example the time interval was .2 seconds.

The algorithm assumes that a reflector exists at each such zero-offset time. If there are large semblance values in a time plane, that "reflector" will have a strong influence on the solution. If there are only small semblance values, the reflector will have little influence on the solution. The tick marks on the right side of Figure 3.8 show the location of the five time planes used in this example. Because of the short cable length (see top of Figure 3.8), these shallow reflectors provide most of the information about the low velocity anomaly's distribution in depth.

The starting model for the iterative ascent algorithm is shown in Figure 3.9. The model consists of thirteen layers; five are above the shallowest reflector. The laterally-invariant interval velocities shown in Figure 3.9 were derived with the one-dimensional

algorithm of the last chapter, at a midpoint that was clearly away from the anomaly. By making the model have more layers than reflectors, the velocity analysis algorithm allows for depth variation of the velocities between the reflectors.

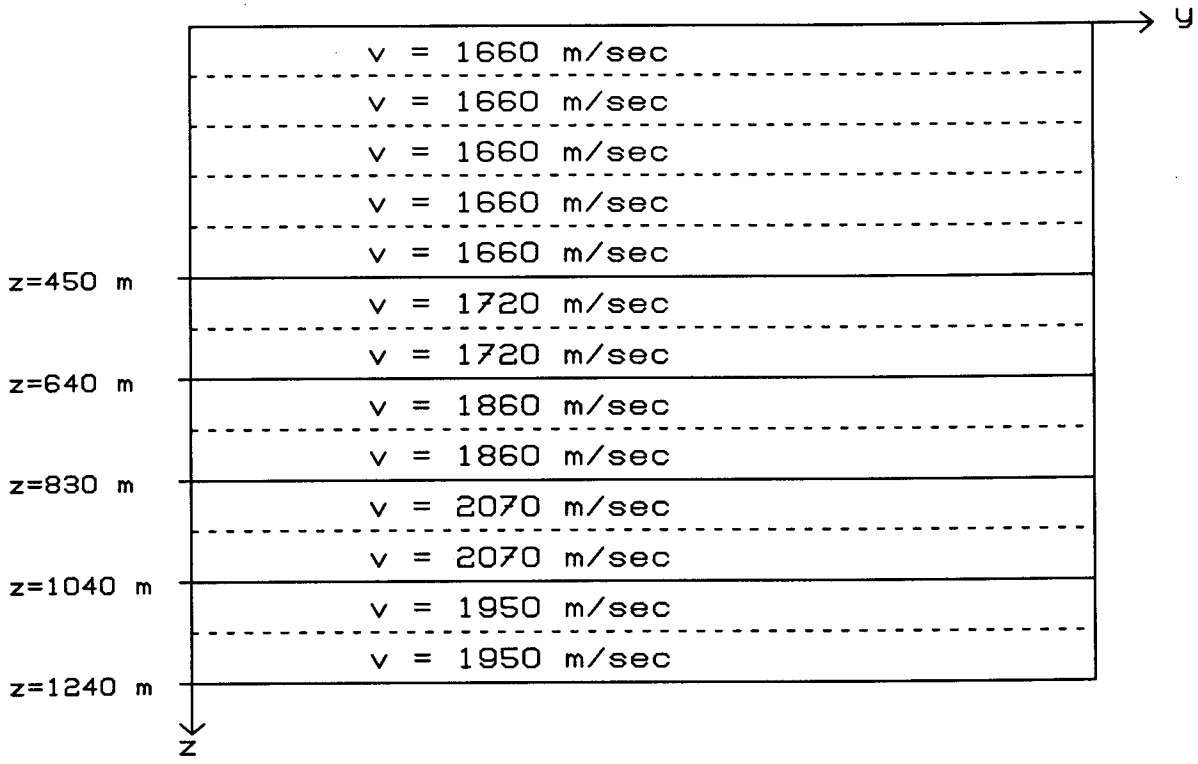

FIG. 3.9. The starting model for the ascent algorithm. The model has thirteen layers. The solid lines show the locations of the reflectors that supplied the stacking slownesses.

Figures 3.10 and 3.11 show contour plots of semblance as a function of stacking slowness and midpoint, for the time planes that I used in the velocity analysis. The reflectors are at times .55, .75, .95 (Figure 3.10), 1.15, and 1.35 sec (Figure 3.11). The straight line through each of the planes shows the stacking slownesses of the starting model. Because this starting model is laterally invariant, its stacking-slowness curves are straight lines. The strong lateral variation of the stacking slownesses is clearly visible in all five planes.

Figures 3.10 and 3.11 also show the stacking slownesses corresponding to the successive models in the iterative process; these are the series of curved lines, which clearly move towards the peaks of semblance as the iterations progress. Applied to this example, the algorithm converges after twenty iterations. Note however, that the stacking

slowness curves do not exactly reach the peaks. The following section shows this to be due to the damping effects of the model penalty-function.

The derived interval-slowness model is shown in Figure 3.12; it actually shows the change in the interval slowness from the starting model to the final model. Clearly visible is a large shallow anomaly, a positive slowness (low velocity) anomaly. The maximum value of the anomaly is .09 s/km, which is about 15% above the background values. This shallow anomaly is responsible for the complicated, laterally varying stacking slowness seen at all times in Figures 3.10 and 3.11.

A closer inspection of figure 3.12 reveals additional features. Particularly interesting is the way the anomaly shifts slightly to the right with increasing depth. This asymmetry suggests that the vertical smearing of the anomaly is not simply due to poor vertical resolution. Another interesting feature is the slight broadening of the anomaly immediately above the shallowest reflector (e.g. at midpoint 2 km, depth .35 km). Large-offset raypaths traveling through the center of the anomaly also travel through this region. The inversion tends to smear the anomalous slowness along these raypaths; this broadening is a typical form of backprojection artifact.

Model penalty function

Just as in the one-dimensional case of the previous chapter, the weight given to the model penalty-function can strongly influence both the derived model and the fit to the data. The lateral smoothness due to the $\mathbf{D_y}^T \mathbf{D_y}$ term in equation (3.11) is clearly visible in Figures 3.10, 3.11 and 3.12. If this term were not present, the stacking-slowness curves would follow the details of the peaks closely; instead, they smoothly follow the general trend. Note once again that this smoothness comes from the model; the data (the semblance planes) are certainly not smooth.

The smoothness in depth, due to the $\mathbf{D_z}^T \mathbf{D_z}$ term in equation (3.11), is evident in figure 3.12. Because there are several layers between each pair of reflectors (see figure 3.9), the most important effect of this smoothness term is to "tighten" the model between reflectors. An extreme version of this "tightening" would be achieved if a model was used that had only one layer between each pair of reflectors. This extreme case would, however, not allow the clear decrease in amplitude with depth of the anomaly seen in figure 3.12.

Further effects of the model penalty-function can be seen in Figures 3.13, 3.14 and 3.15. Figure 3.13 shows the event velocity analyses for the shallowest and deepest events (times of .55 and 1.35 seconds). Superposed on each are the stacking-slowness curves

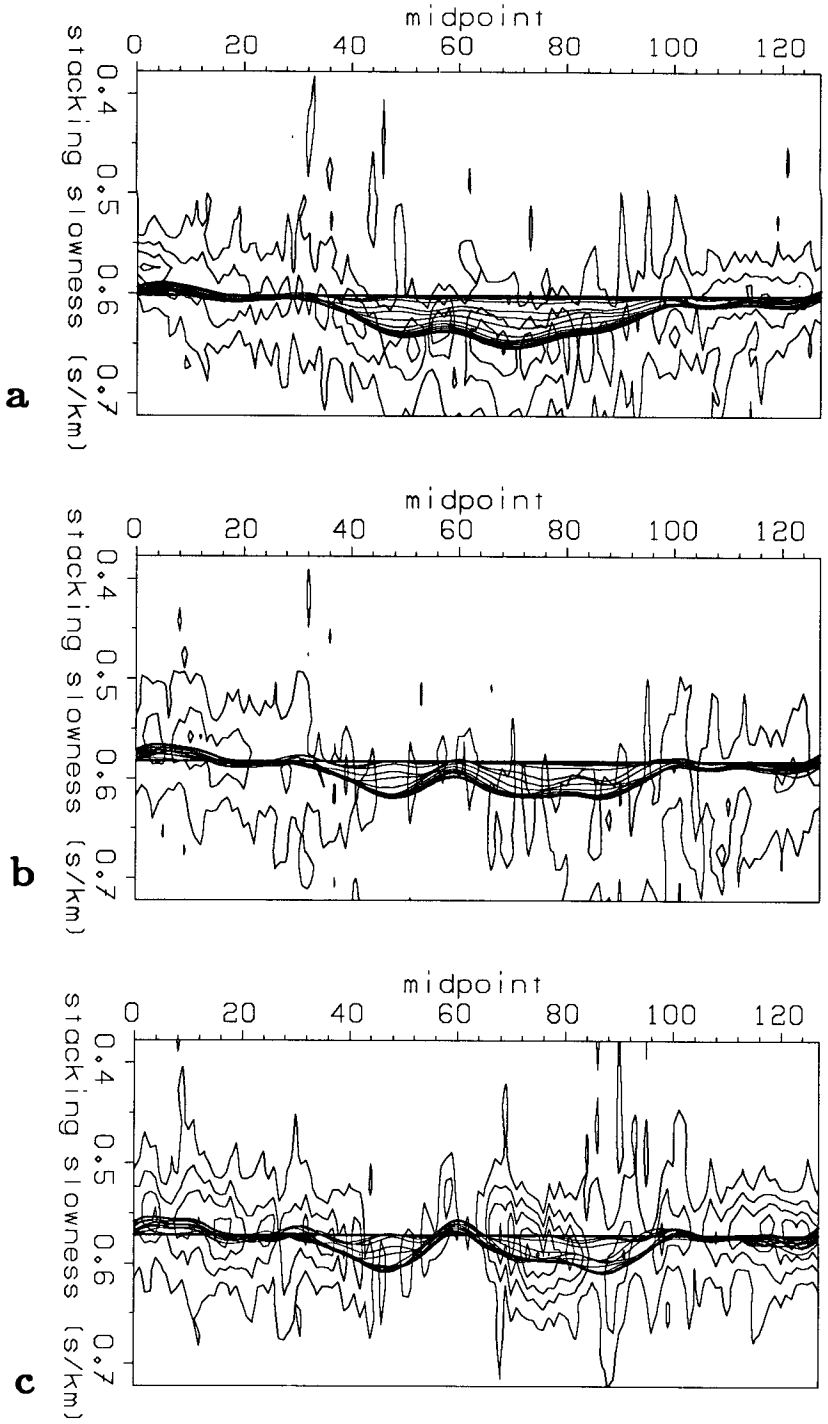

FIG. 3.10. Contour plots of semblance as a function of stacking slowness and midpoint, for the reflectors at times: a) .55 sec, b) .75 sec, c) .95 sec. The straight line through each of the planes is the stacking slowness corresponding to the starting model. The other lines through each of the planes are the stacking slownesses corresponding to the successive models in the iterative process.

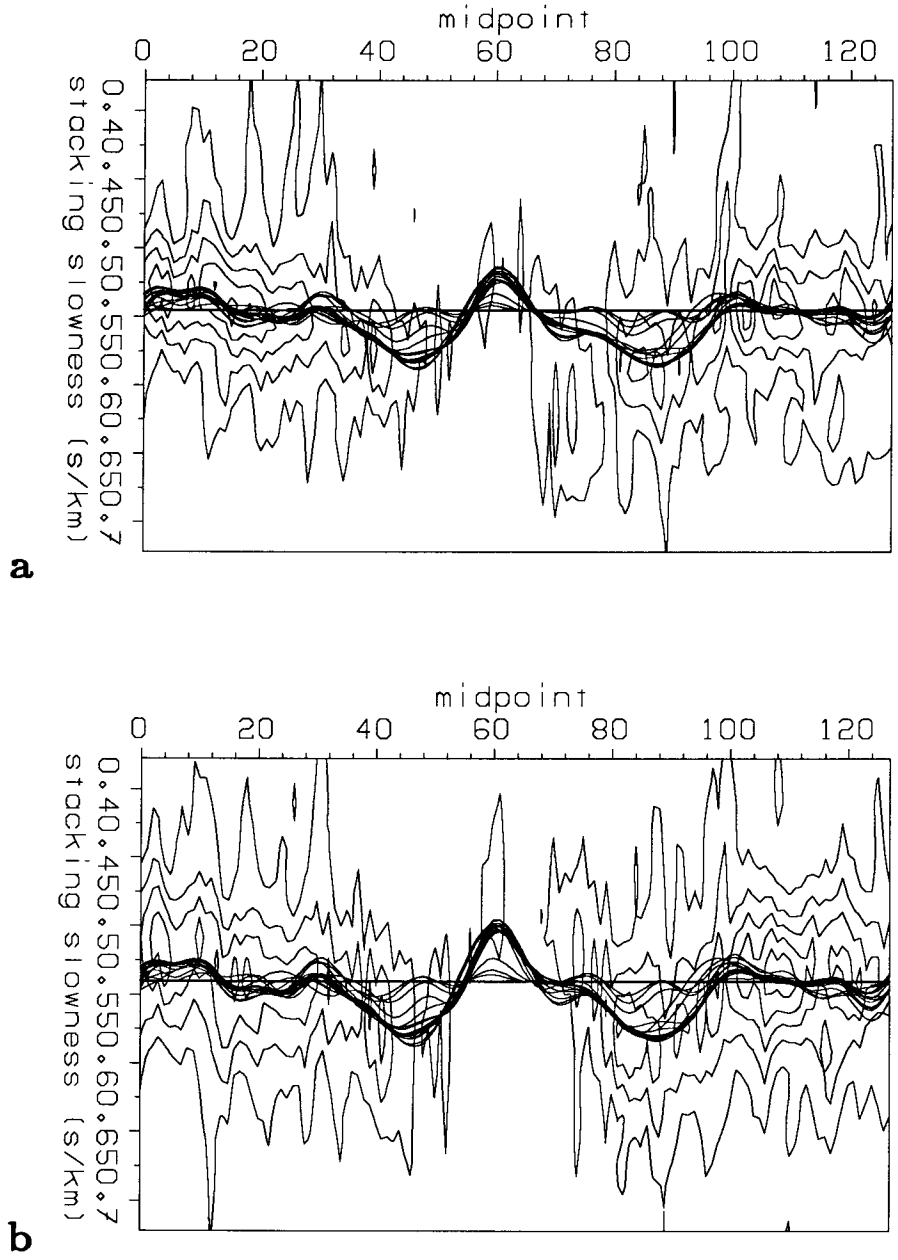

FIG. 3.11. Contour plots of semblance as a function of stacking slowness and midpoint, for the reflectors at times: a) 1.15 sec, and b) 1.35 sec. The straight line through each of the planes is the stacking slowness corresponding to the starting model. The other lines through each of the planes are the stacking slownesses corresponding to the successive models in the iterative process.

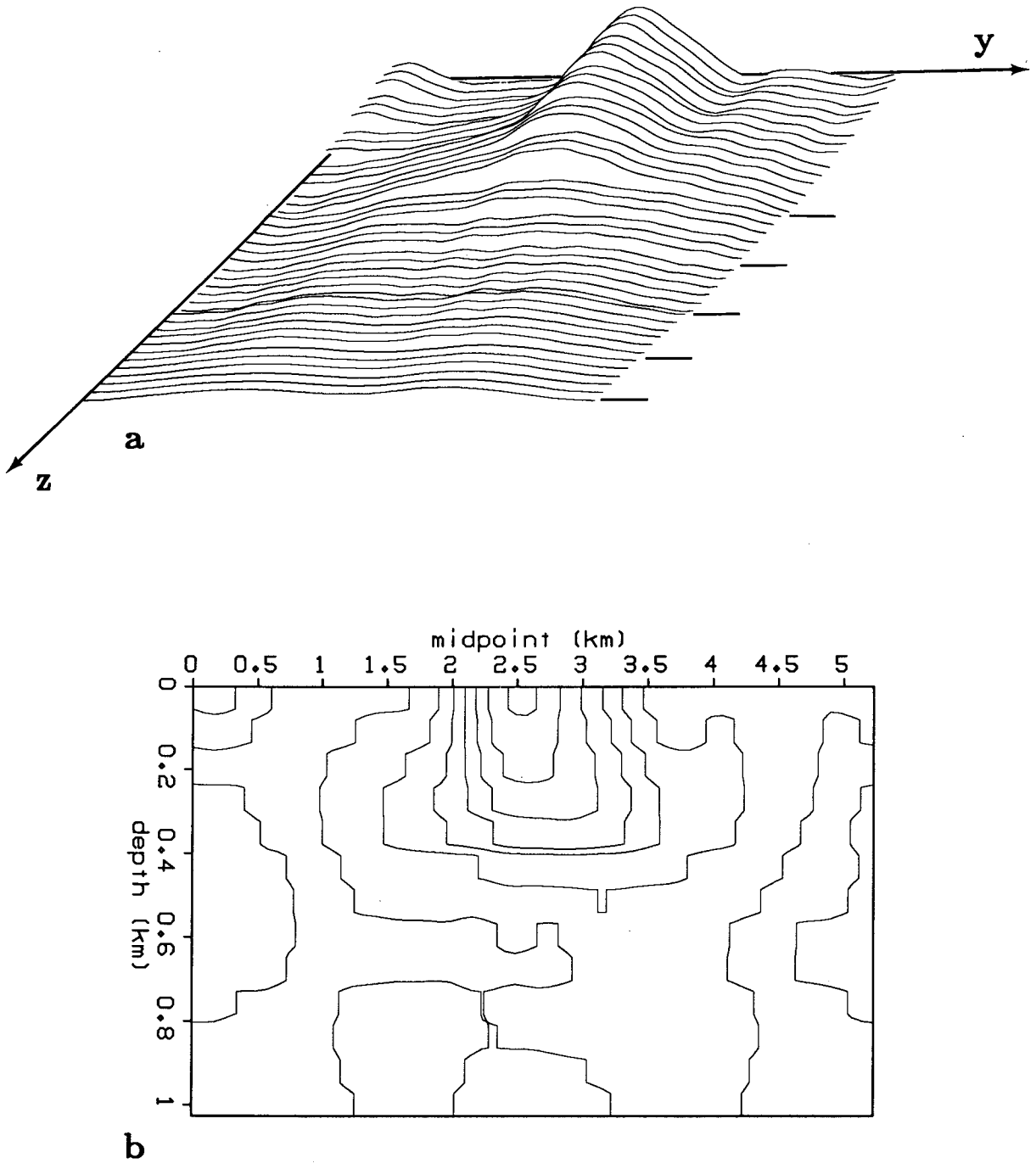

FIG. 3.12. Interval slowness model. a) Hidden line plot of change in interval slowness from starting to final model. b) Contour plot of change in interval slowness from starting to final model. Note the large, shallow, positive slowness (low velocity anomaly).

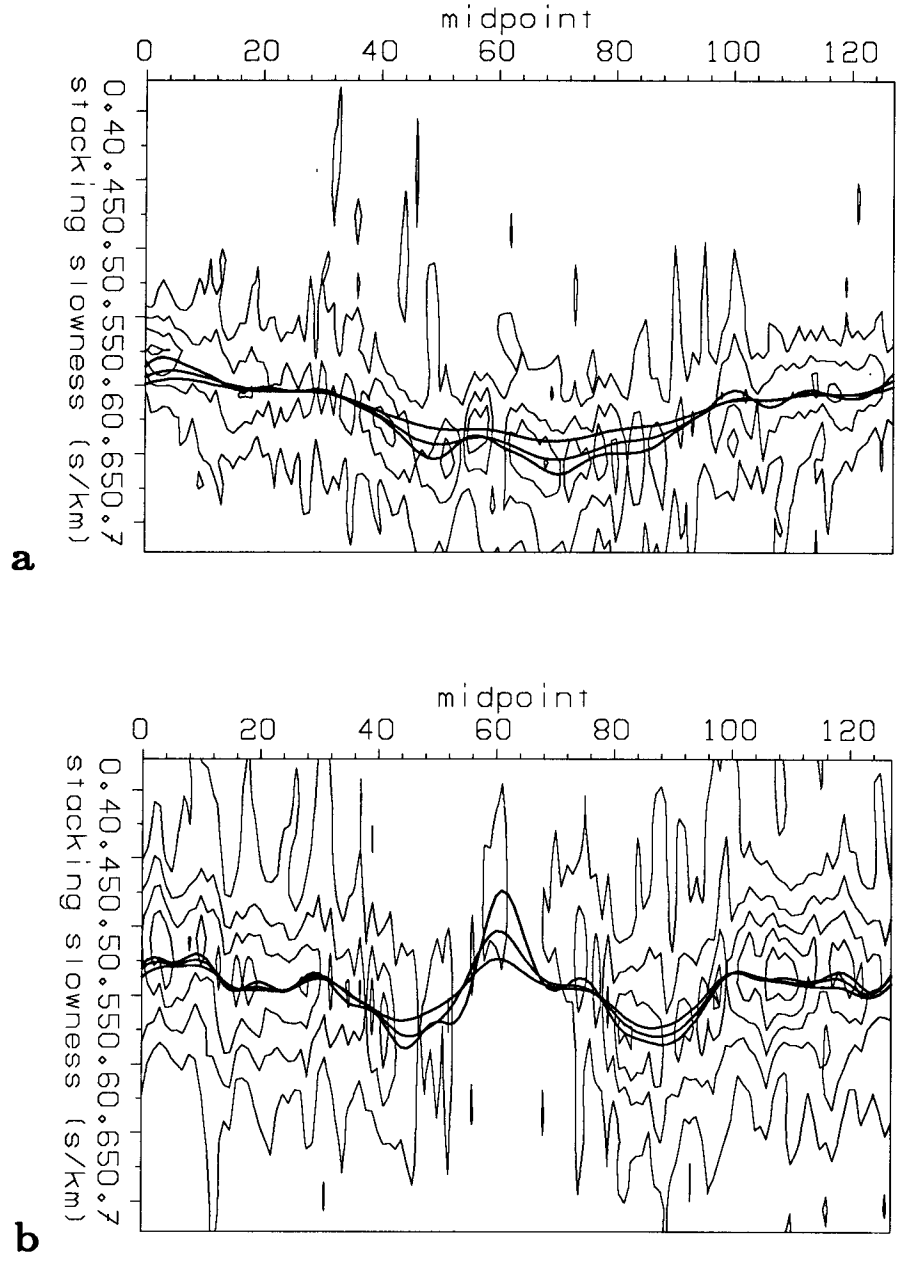

FIG. 3.13. Contour plots of semblance as a function of stacking slowness and midpoint, for the reflectors at times: a) .55 sec, b) 1.35 sec. The lines through each of the planes are the stacking slownesses corresponding to the final iterations of models with varying weight for the model penalty function. The models with the heaviest weight on the penalty function produce the stacking-slowness curves that are farthest from the peaks.

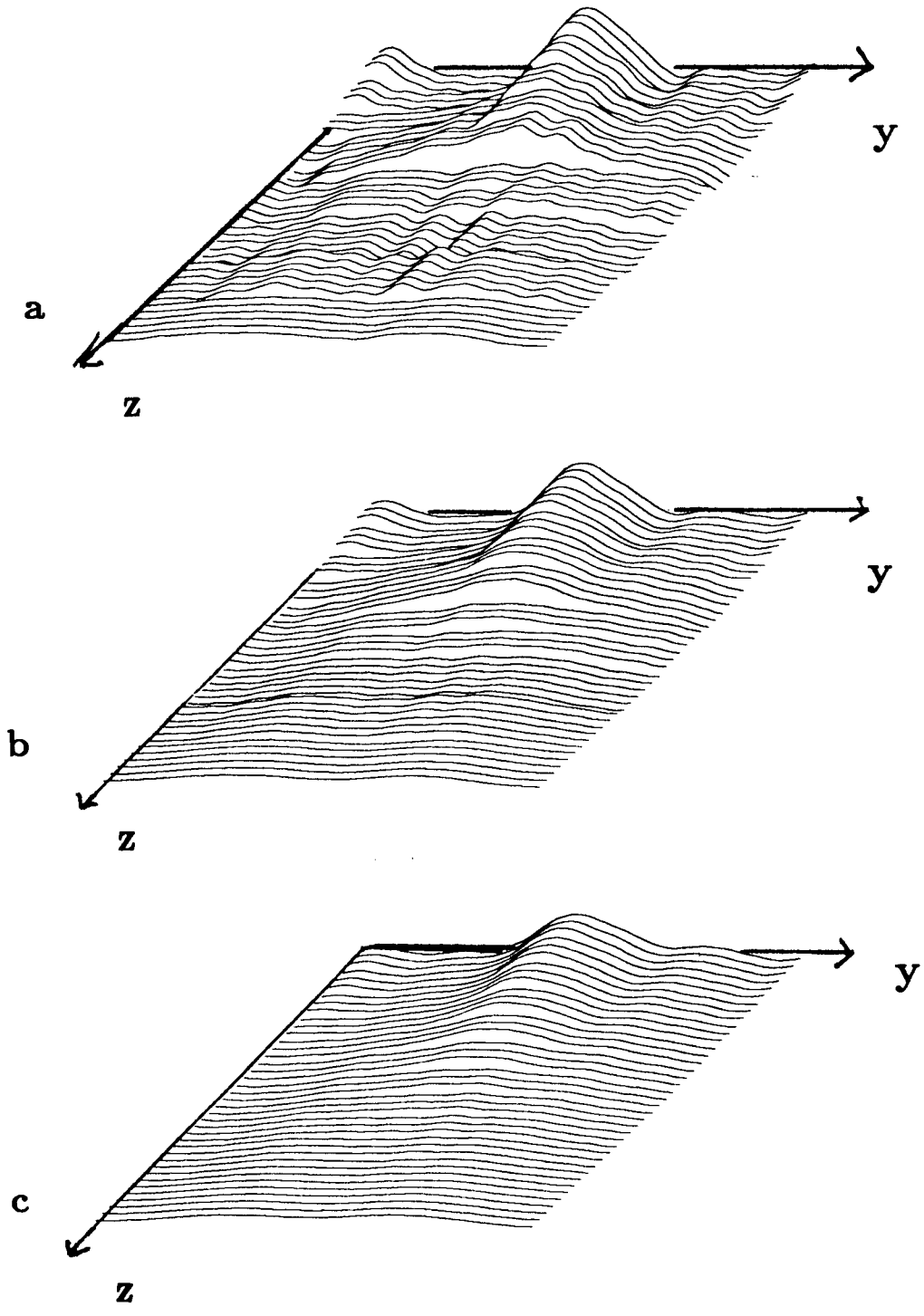

FIG. 3.14. Hidden line plots of the slowness models derived with varying amounts of damping. This figure shows the change from the starting model to the final model. a) Model A; weak damping. b) Model B; moderate damping (same model as Figure 3.12). c) Model C; strong damping.

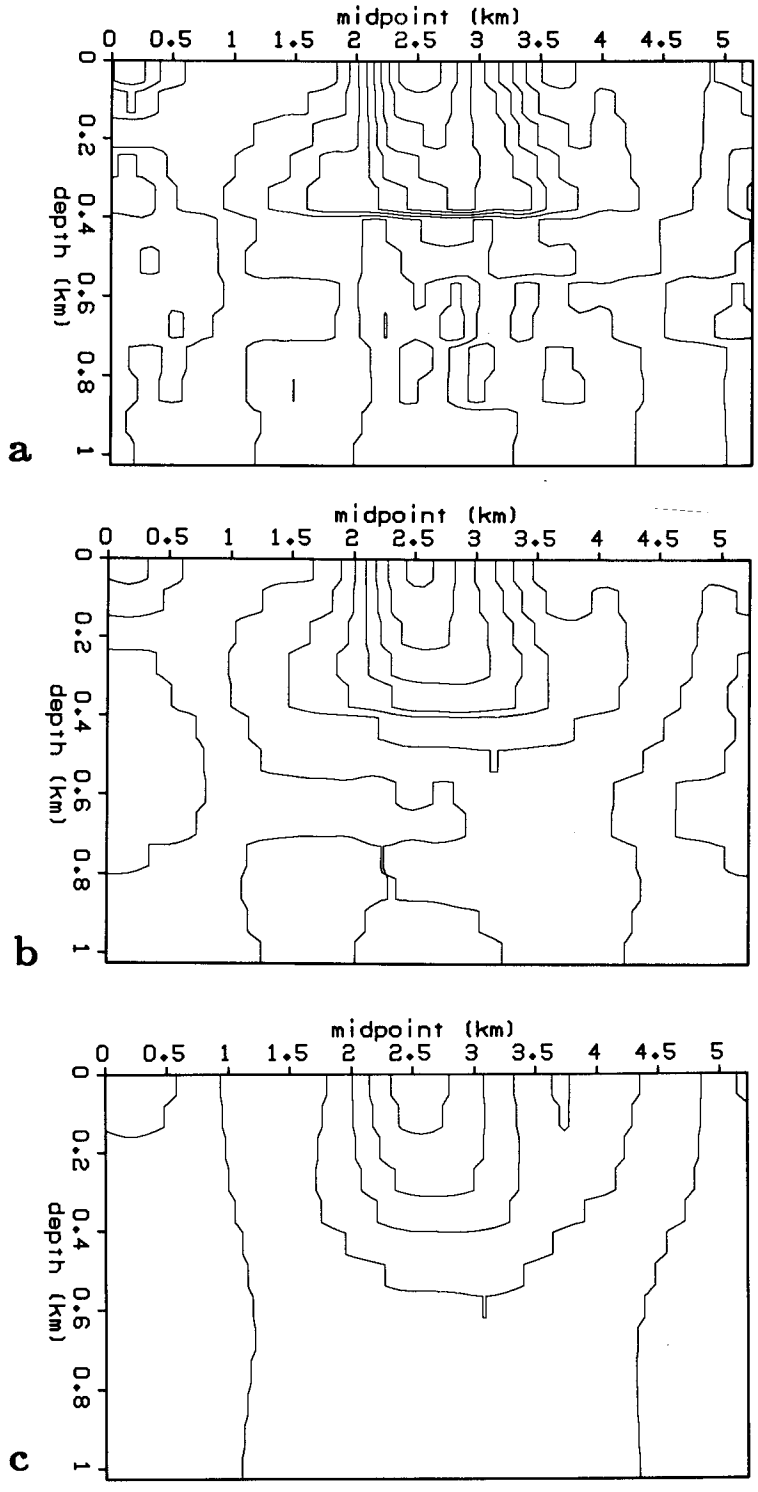

FIG. 3.15. Contour plots of the slowness models derived with varying amounts of damping. This figure shows the change from the starting model to the final model. a) Model A; weak damping. b) Model B; moderate damping (same model as Figure 3.12). c) Model C; strong damping.

corresponding to models with varying weights of the model penalty-function. The stronger the weight, the further the curves of Figure 3.13 are from the peaks. Thus, the model penalty function provides a form of damping to the solution. The model that was shown in Figure 3.12 produced the intermediate curve for each event.

Figure 3.14 shows the interval slowness models: (a) is the model with the weakest penalty weight, (c) the strongest. Figure 3.14b shows the model of Figure 3.12 for comparison. Contour plots of the same three models are shown in Figure 3.15. These three models will be referred to as models A, B and C for the remainder of this chapter. The penalty weight increased by a factor of 10 from model A to B, and again by 10 from B to C.

Increasing the penalty weight clearly produces a smoother model. The lateral smoothness is evident in the absence of short wavelength features in model C. The smoothness in depth is evident in the way that the shallowest reflector provides less of a lower bound to the anomaly in the smoothest model (C) than in the least smooth model (A). As shown in figure 3.13, however, a very smooth model fits the data poorly. This situation is familiar in inverse problems: there is a trade-off between reliability of the model, and quality of fit to the data. Model B thus represents a compromise between the two extreme cases of Models A and C.

3.6 FIELD DATA EXAMPLE: REMOVING TRAVELTIME EFFECTS OF ANOMALY

The previous section showed a series of interval slowness models that were discussed in terms of two criteria: the reasonableness of the model, and the quality of the fit to the data. The quality of the fit to the data can also be studied in a second way: instead of looking only at the stacking slownesses predicted by the model, look also at the predicted traveltimes. This second way of studying the results is important: a reasonable interval slowness model must be able to explain the laterally varying traveltimes as well as the stacking slownesses.

This section studies the laterally varying traveltimes predicted by the model through a series of traveltime corrections. That is, after removal of the traveltimes predicted by the laterally varying part of the model, the traveltimes of the remaining data should be laterally invariant. These traveltime corrections can be easily calculated with the help of a linear theory.

Linear traveltime theory

Fermat's principle provides the means for the calculation of traveltime perturbations due to a perturbation in interval slowness (Δw_{in}). This principle allows the perturbation in traveltime to be calculated as the integral of the anomalous slowness, along the raypaths determined by the background velocity (Aki and Richards, 1980). That is:

$$\Delta t \approx \int_{S_0} \Delta w_{in} \, dS_0 \, .$$

where S_0 represents the ray corresponding to the background velocity.

For the flat reflectors and laterally invariant background of this example, the background raypaths are easily calculated. From Figure 3.16:

$$\Delta t\,(y\,,\,x\,,\,z\,,\,z_a\,) \;=\; \left[\Delta w_{in}\,(y-\mu,\,z_a\,)+\Delta w_{in}\,(y+\mu,\,z_a\,)\right]\frac{dz_a}{\cos\theta} \qquad (3.12)$$

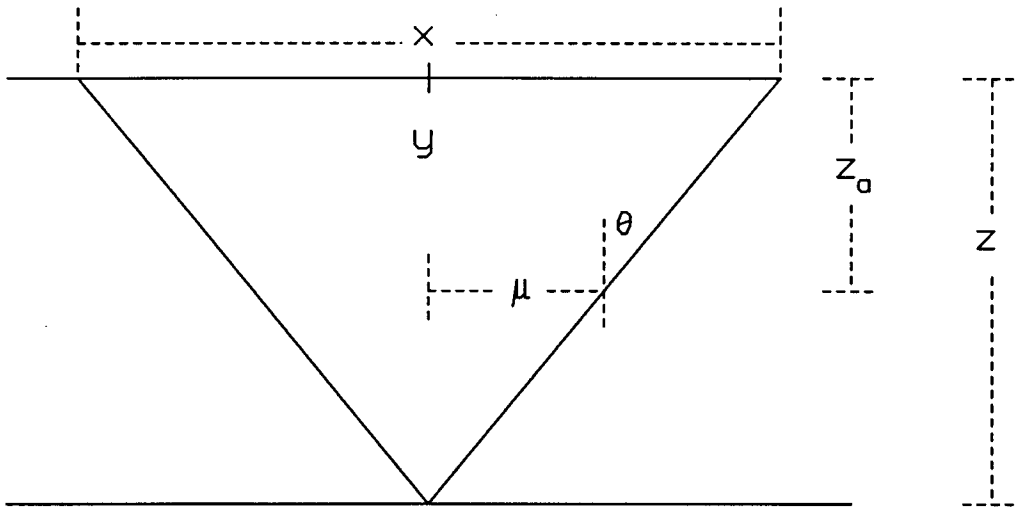

FIG. 3.16. Diagram of the raypath to the reflector at depth z, for offset x. The raypath is drawn for a depth variable velocity. μ is the lateral distance of the raypath from y, when it is at depth z_a.

μ is the lateral distance of the raypath from the midpoint y, and θ is the angle that the ray makes with the vertical, when the ray is at depth z_a. As shown in figure 3.16, μ and θ depend on the background raypath. This dependence can be expressed by means of the ray parameter ($p = \sin\theta/v$). Specifically,

$$\cos\theta(x, z, z_a) = \left[1 - p^2 v^2(z_a)\right]^{1/2}, \tag{3.13}$$

and

$$\mu(x, z, z_a) = \int_{z_a}^{z} \frac{pv(\varsigma)}{\left[1 - p^2 v^2(\varsigma)\right]^{1/2}} \, d\varsigma . \tag{3.14}$$

For a constant-velocity background, equations (3.13) and (3.14) take the much simpler form:

$$\cos\theta = \frac{z}{\left[\left(\frac{x}{2}\right)^2 + z^2\right]^{1/2}},$$

and

$$\mu = \frac{x}{2} \frac{(z - z_a)}{z} .$$

Accumulating the effects from the entire raypath leads to

$$\Delta t(y, x, z) = \int_0^z \left[\Delta w_{in}(y - \mu, z_a) + \Delta w_{in}(y + \mu, z_a)\right] \frac{dz_a}{\cos\theta} . \tag{3.15}$$

For the constant-velocity case, the Fourier transform over midpoint of equation (3.15) gives

$$\Delta t(k_y, x, z) = \int_0^z \Delta w_{in}(k_y, z_a) \cos k_y x \, \frac{dz_a}{\cos\theta} , \tag{3.16}$$

(Kjartansson, 1979). Introducing the Fourier transform of Δw_{in} has simplified the integral. More importantly, equation (3.16) now expresses the model specifically in terms of the parameters of the inversion: thin strips in depth and sinusoids laterally. Thus the evaluation of equation (3.16), followed by an inverse Fourier transform over midpoint wavenumber, leads to the traveltime perturbations corresponding to the anomalous interval slownesses.

Static shifts

A special case of equation (3.16)—static shifts—provides an interesting first check of the results. Because the maximum offset is limited, the raypaths for the deep reflectors have a steep propagation angle. Refraction in the low-velocity near-surface further steepens these raypaths. Because of the shallowness of the anomalous material, most of the traveltime delay for the deep reflectors will take the form of static shifts. Thus, the traveltime delays predicted by equation (3.16), under the assumption of vertical raypaths, can be directly compared to the results of a residual-statics program. This comparison provides an independent check on the interval slowness models derived from stacking slownesses.

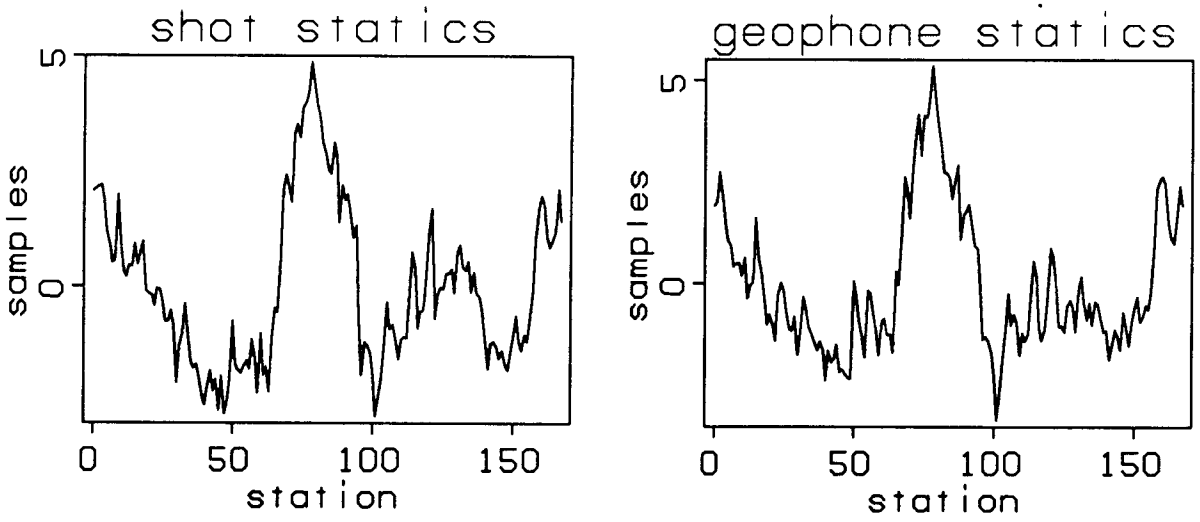

FIG. 3.17. Shot and geophone statics derived from residual-statics program (Ronen and Claerbout, 1985).

Figure 3.17 shows the shot and geophone statics derived from a residual-statics program (Ronen and Claerbout, 1985). The time gate went from 3.5 to 4 seconds, the part of the data that best satisfied the conditions needed for there to be vertical raypaths in the near surface. The long-wavelength component of these statics can be compared with the traveltime delays predicted by the near-surface (i.e. the layers above the first reflector) of the interval-slowness model, if vertical raypaths are assumed

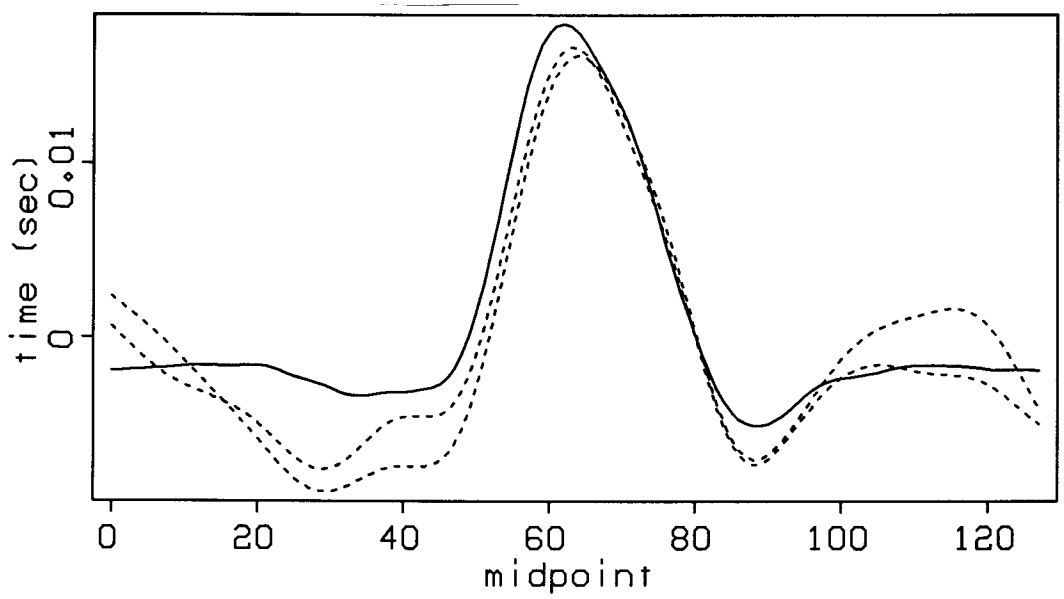

FIG. 3.18. Comparison between long wavelength component of shot and geophone statics of figure 3.17 (dashed lines), and one-way, near-surface delay predicted by interval slowness model (solid line), based on vertical raypaths in near surface. The curves are very similar.

($\Delta t = \Delta w_{in}\, z$). As shown in figure 3.18, the curves are quite similar. This similarity provides an independent confirmation of the magnitude and lateral extent of the derived interval slowness model.

Figure 3.19 shows stacked sections made with and without the static corrections of figure 3.17. The deep portion of the data has been properly corrected for the near-surface anomaly. In the shallower parts, the time sag is still visible and the coherence of the stack imperfect. Thus, the more complete offset and time dependence of equation (3.16) is required to fully remove the effects of the time sag. Furthermore, this offset dependence will provide a means by which the distribution in depth of the interval slowness anomaly can be studied.

Dynamic corrections applied

The consideration of static corrections showed that the magnitude and lateral extent of the anomaly is consistent with the laterally varying traveltimes of the deep part of the data. The distribution in depth of the anomaly can be studied if the dynamic corrections of equation (3.16) are used. Figure 3.20 shows two versions of the same constant-offset section: 3.20a contains the uncorrected data; 3.20b contains the

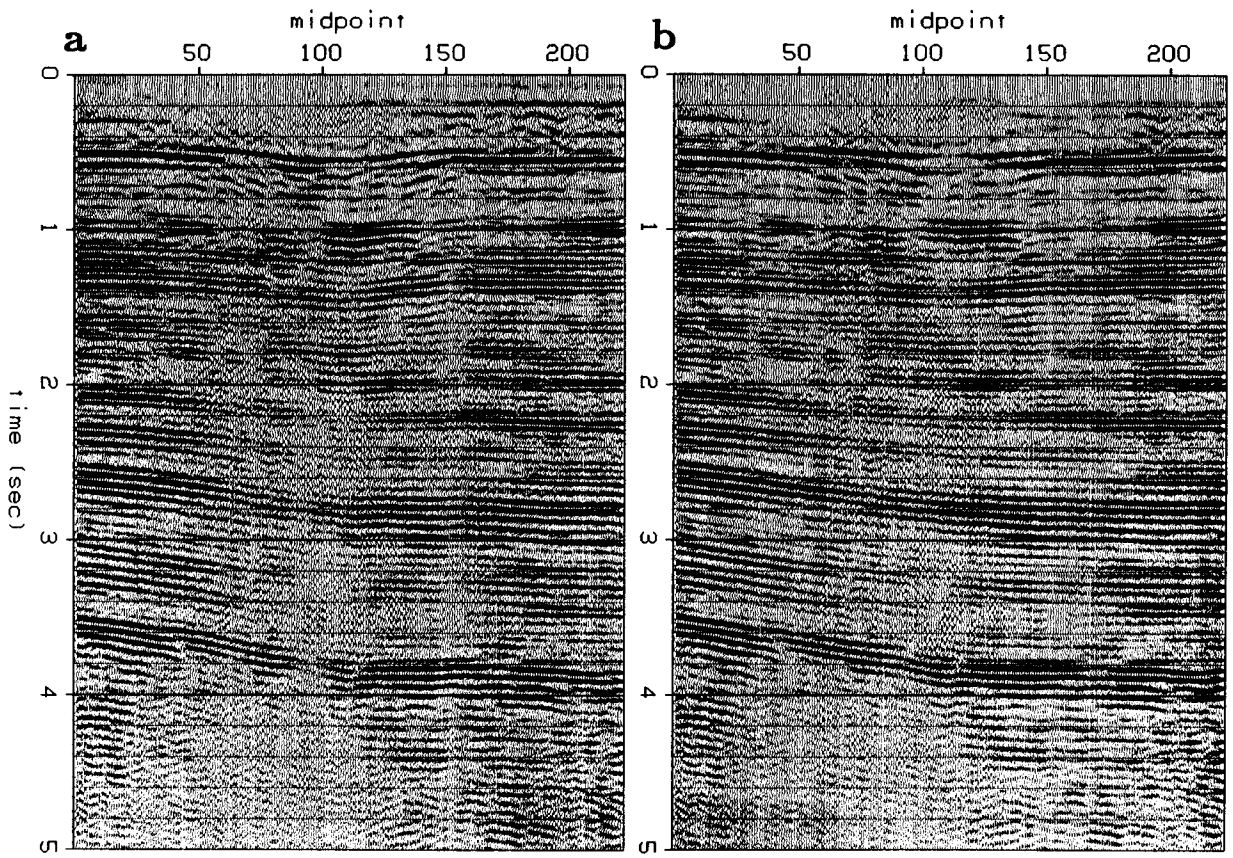

FIG. 3.19. a) Stack without static corrections. b) Stack with static corrections. Note the improved continuity in the deep part of the data, provided by the static corrections. Note also that the static corrections have been unable to properly correct the shallow part of the data.

data after removal of the anomalous traveltimes due to the near-surface part of Model B (the interval-slowness model of figure 3.14b). The reason for the use of only the near-surface part of the anomalous model will be discussed in a moment. The offset in Figure 3.20 is 330 meters. Figures 3.21 and 3.22 also compare corrected and uncorrected data, but for offsets of 660 and 1100 meters. The time sag is quite dramatic in the uncorrected data, and has mostly been removed by the dynamic corrections. Because the traveltime corrections of equation (3.16) are based on the assumption of straight ray-paths, one would expect the corrections to be only approximately correct. Figures 3.20, 3.21 and 3.22 show that the interval slowness model not only explains the laterally varying stacking slownesses: it also explains the laterally varying traveltimes.

The traveltime corrections applied to Figures 3.20, 3.21, and 3.22 were based on the near-surface part of the interval slowness model, that is, the part above the shallowest reflector. This shallow part seems to contain most of the anomaly (see Figure 3.14b).

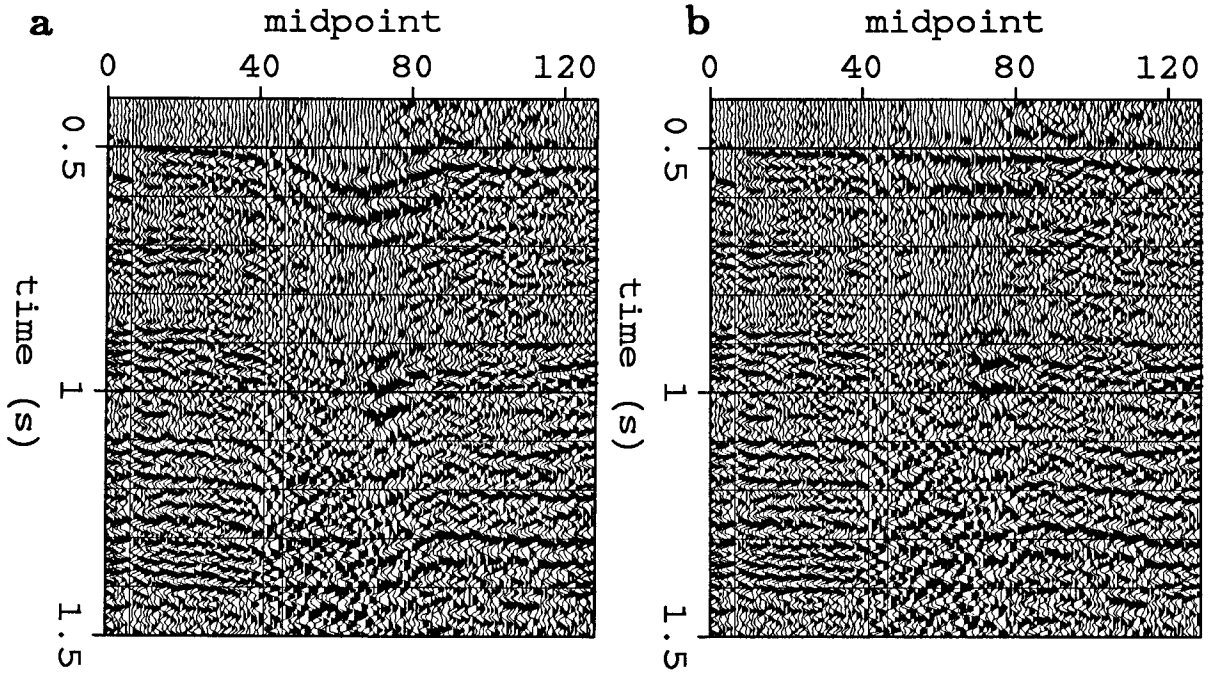

FIG. 3.20. Constant-offset sections for offset = 330 meters. a) uncorrected. b) corrected according to Model B (shown in figure 3.14b). The corrections have effectively removed the time sag.

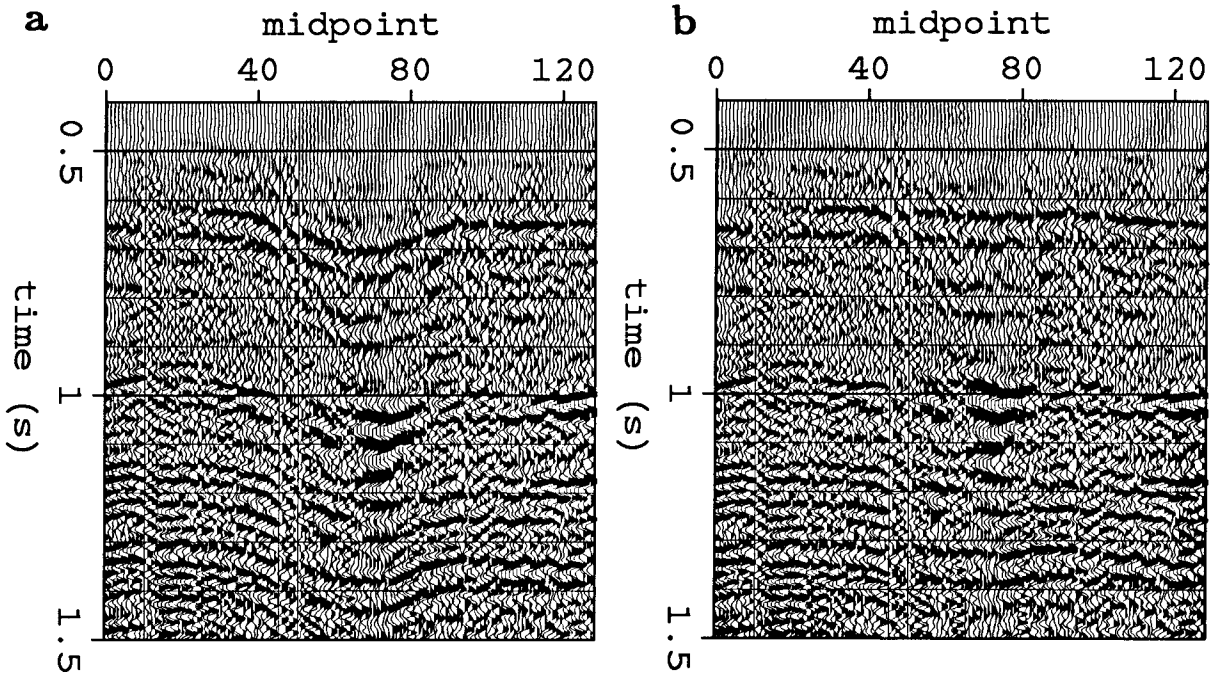

FIG. 3.21. Constant-offset sections for offset = 660 meters. a) uncorrected. b) corrected according to Model B.

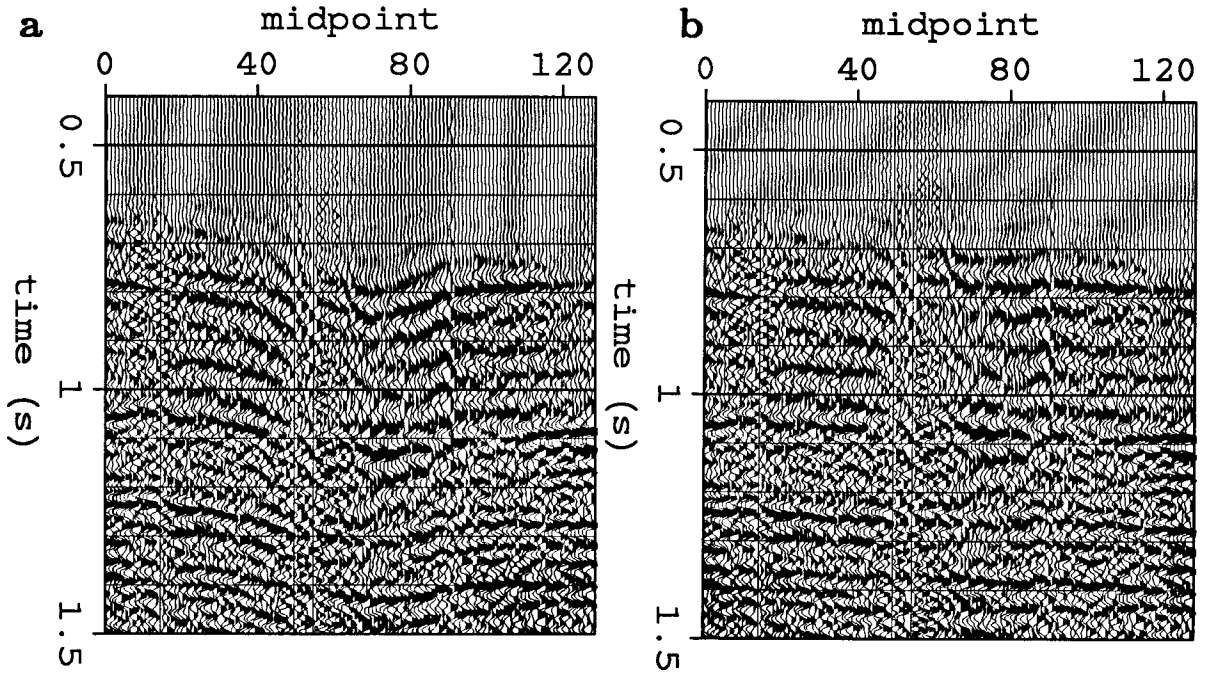

FIG. 3.22. Constant-offset sections for offset = 1100 meters. a) uncorrected. b) corrected according to Model B.

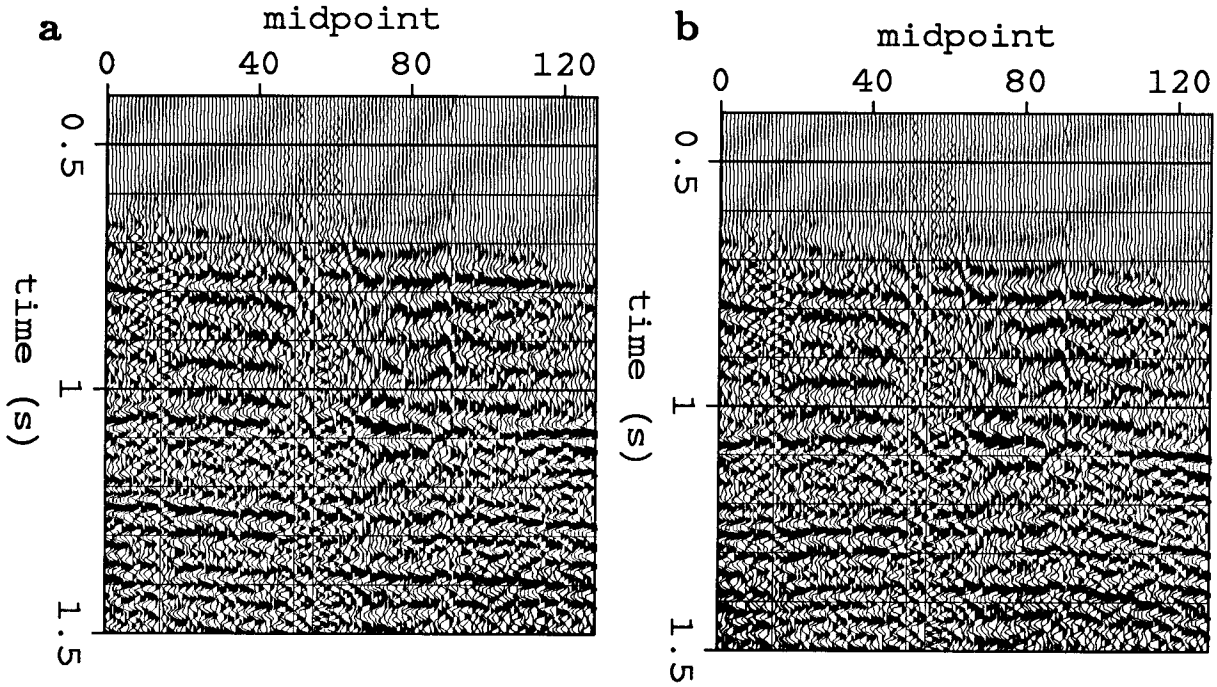

FIG. 3.23. Constant-offset sections for offset = 1100 meters. a) corrected according to only the near-surface part of the interval slowness model (same as figure 3.20b). b) corrected according to the full model. The shallow parts of the two sections are identical. Note in (b) the pull-up of the deep reflectors beneath midpoint 90.

Unfortunately, applying the traveltime corrections due to the low amplitude, deep part of the model leads to clearly incorrect results. Figure 3.23 shows these results, for offset = 1100 m; for comparison it repeats the data corrected according to only the near-surface part of the model. The shallow parts of the two sections are, of course, the same. The deep reflectors of the fully corrected data (b) show a pull-up in time; the nearly sinusoidal interval slownesses of the deep part of Model B (see Figures 3.14b and 3.15b) are responsible for this undesirable feature. Thus, although the traveltimes predicted by the well-determined, shallow part of the model are very reasonable, those predicted by the less-well determined deep part of the model are not so reasonable.

3.7 ITERATIVE VELOCITY ANALYSIS AND TRAVELTIME CORRECTIONS

The traveltime correction of Figure 3.23 revealed some problems with the interval-slowness model derived from the stacking slownesses. In particular, the deep, poorly-determined part of the model leads to unreasonable traveltimes. Corrections based on a better-determined model (for example, Model C, of figure 3.14c) could be made, but these corrections would remove only part of the anomaly's effects. On the other hand, if the application of these well-behaved traveltime corrections is followed by a second velocity analysis, the entire model-building procedure can be repeated. Once again, a well-determined model can be built through the use of a large damping factor. In this iterative manner, a well-determined model that fully explains the laterally varying traveltimes can be determined.

This section applies the velocity analysis algorithm of this thesis iteratively. This version of the algorithm loops through the following three steps: first, it calculates the time planes of semblance; second, it uses these semblance values to determine a strongly damped model; third, it applies the traveltime corrections due to the model. The output of the third step becomes the input for the next iteration. In the example that follows, the first iteration is assumed to have produced the heavily damped Model C. Thus, in the second iteration, the semblance planes are computed from data that have been corrected according to Model C.

Figure 3.24 shows the shallowest of these semblance planes, which form the input for the second iteration. For comparison, Figure 3.24 also shows a plane from the same time, calculated on the original data. It is evident that Model C has been able to explain much of the lateral variation in stacking slowness. Nonetheless, some variation remains: this second iteration will try to explain the variation with an interval slowness model.

The results of the second iteration are shown in Figures 3.25 and 3.26. Figure 3.25 shows the shallowest and deepest of the semblance planes, overlaid with the stacking

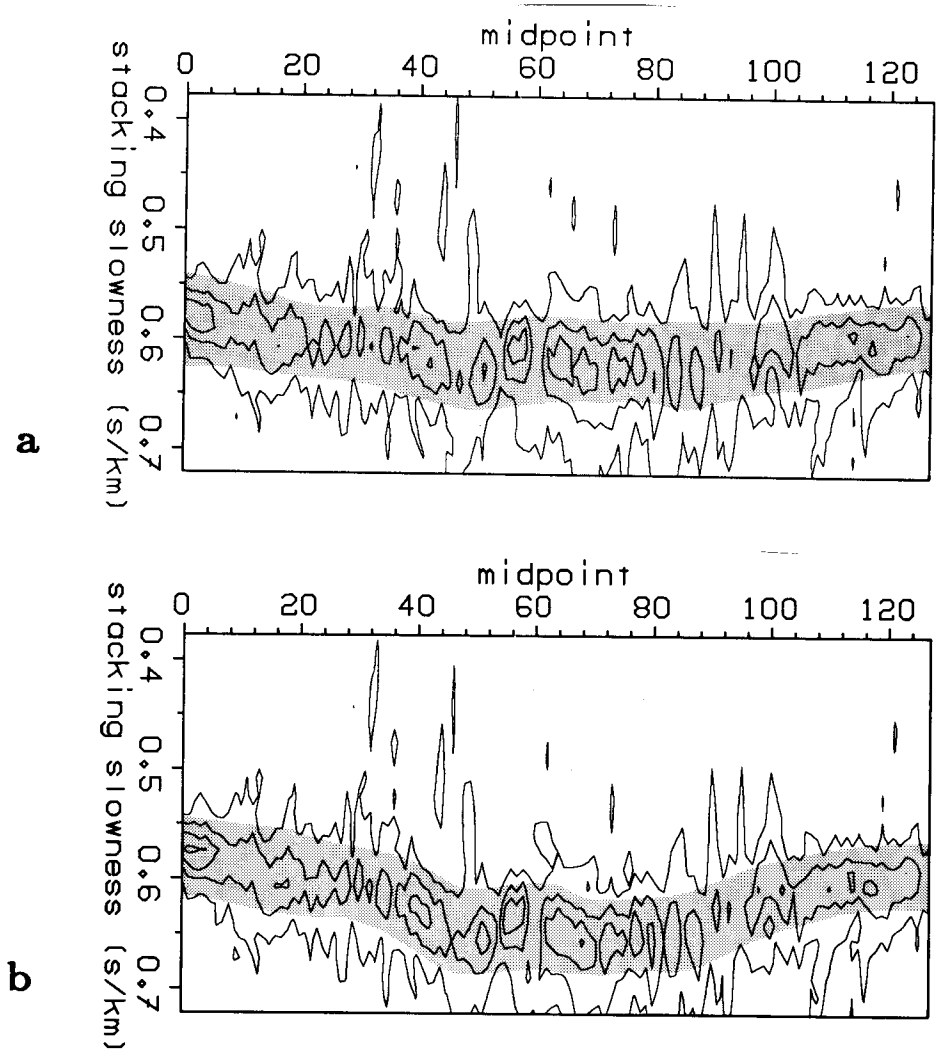

FIG. 3.24. Velocity analysis for reflector at .55 sec. a) After dynamic near-surface corrections, according to the model of Figure 3.14c. b) On raw data. Note the overall decrease in the lateral variation after the corrections.

slowness curves for the successive iterations of the ascent algorithm. Because of the strong damping, the solution has moved only part of the way to the peaks. Figure 3.26 shows the interval slowness model; it is plotted at the same amplitude as the models of figure 3.14. As in the previous iteration (Figure 3.14), a near-surface, positive slowness anomaly has been found.

Next, the traveltime effects of this model can be removed; the resulting data could then go back into the first step to begin another iteration. A constant-offset section of

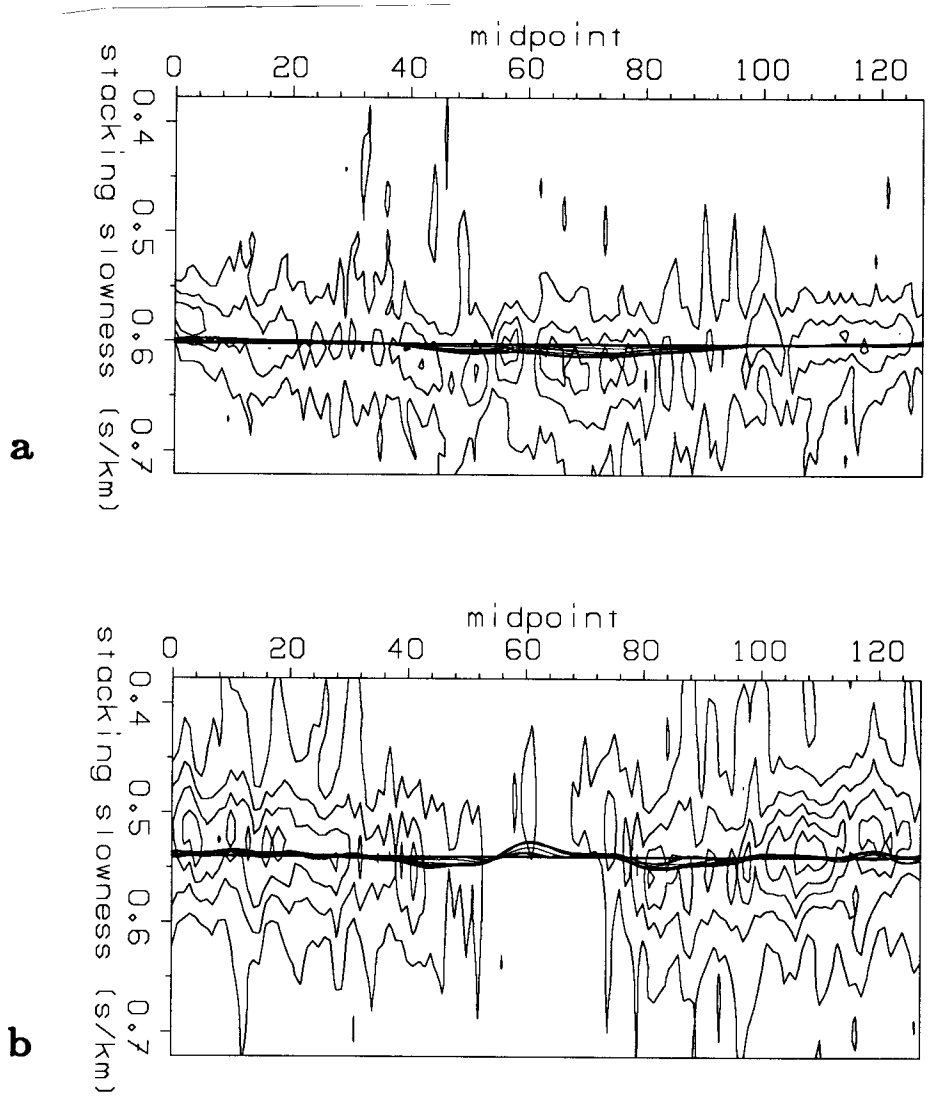

FIG. 3.25. Contour plots of semblance as a function of stacking slowness and midpoint, for the reflectors at times: a) .55 sec, and b) 1.35 sec. The straight line through each of the planes is the stacking slowness corresponding to the starting model. The other lines through each of the planes are the stacking slownesses corresponding to the successive models in the iterative process.

this twice-corrected data is shown in Figure 3.27a (offset = 1100 m). For comparison, the constant-offset section of Figure 3.23b is repeated; these data were corrected according to only the near-surface part of a less strongly damped model (Model B). The net effect on the data of corrections derived through two strongly damped iterations is nearly identical to those derived through a single less strongly damped iteration.

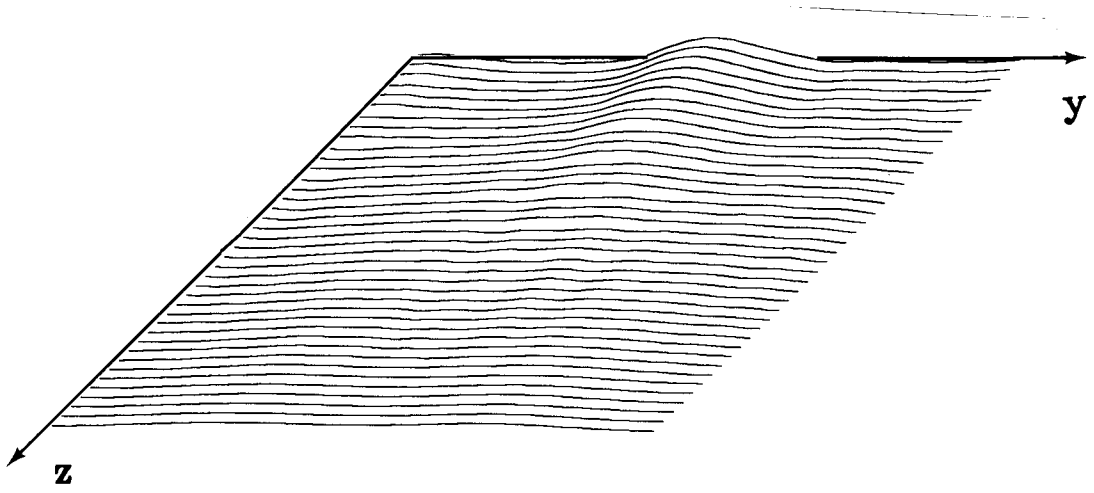

FIG. 3.26. Interval slowness model. This figure shows the change from the starting model to the final model.

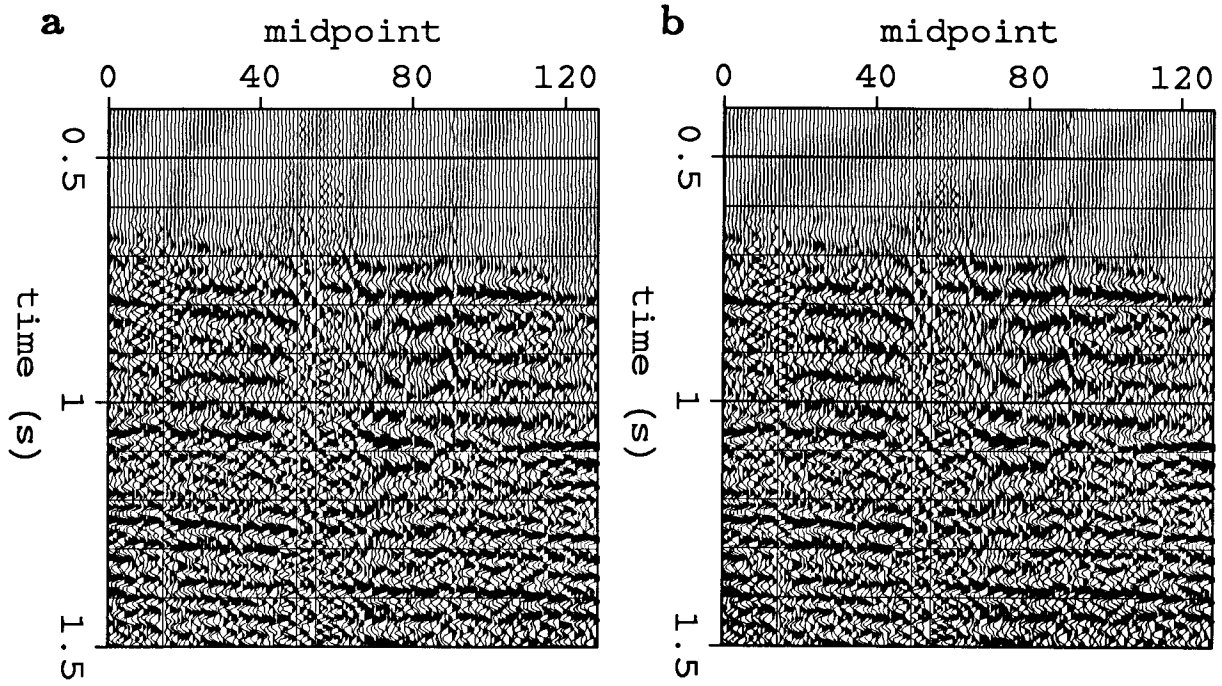

FIG. 3.27. Constant-offset sections for offset = 1100 meters. a) corrected according to a model derived through two iterations. In each iteration the model penalty function was strongly weighted. b) corrected according to only the near-surface part of a less strongly damped interval slowness model (same as figure 3.23b). Even though the models are different, the effect on the data is nearly identical.

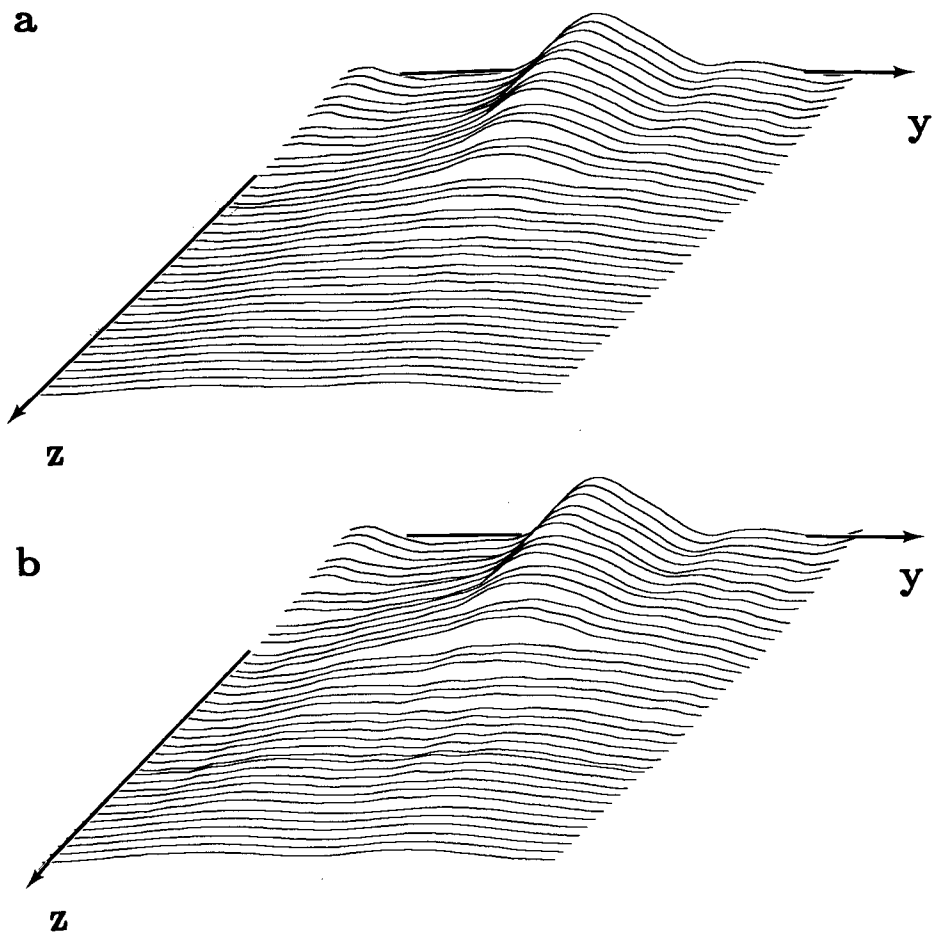

FIG. 3.28. a) Hidden line plot of total anomalous model derived through two iterations. In each iteration the model was strongly damped. b) Hidden line plot of model derived in one iteration with less damping. The model derived in two iterations is smoother.

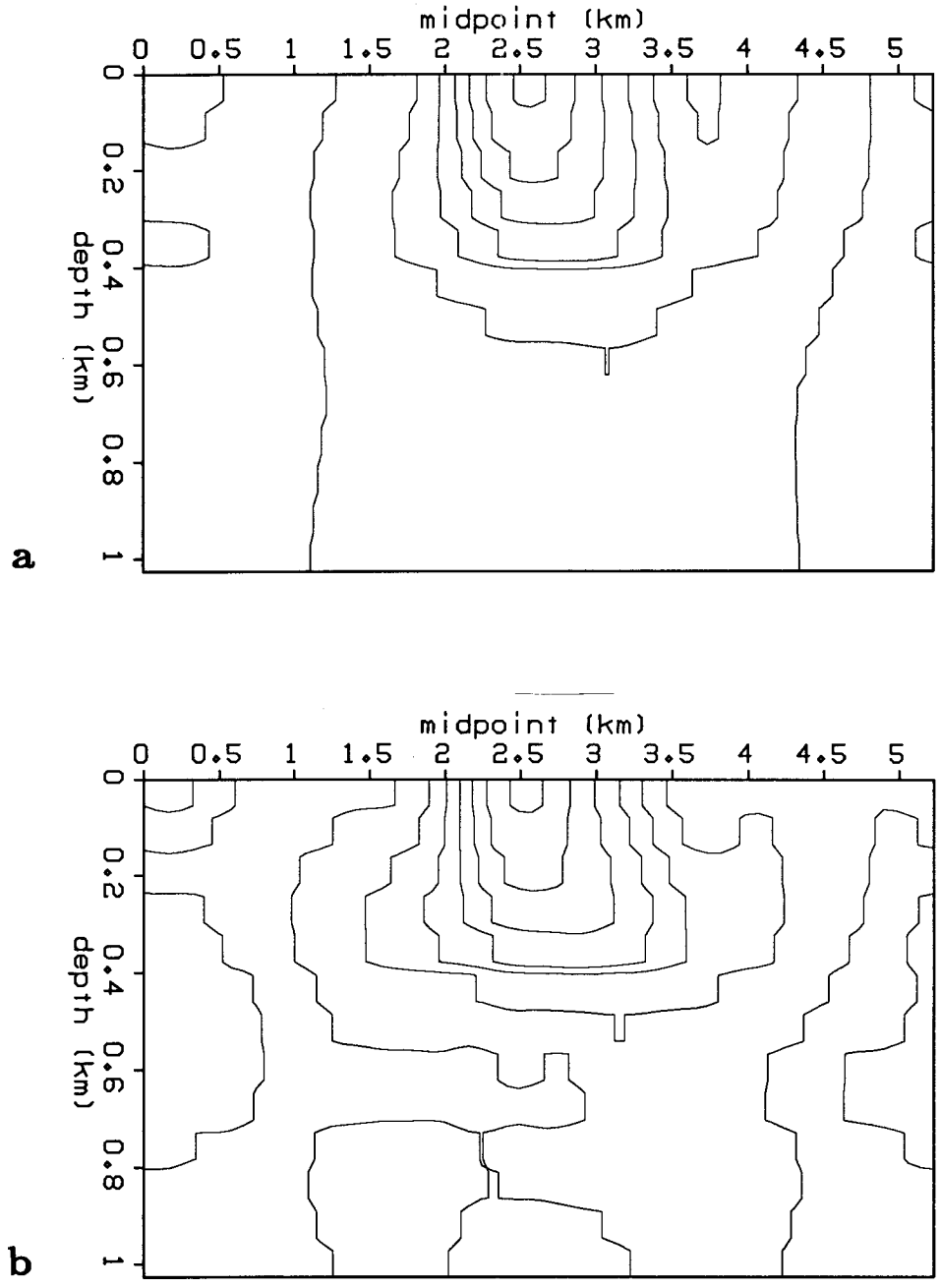

FIG. 3.29. a) Contour plot of total anomalous model derived through two iterations. In each iteration the model was strongly damped. b) Contour plot of model derived in one iteration with less damping. In addition to being generally smoother, the model derived in two iterations is narrower immediately above the shallowest reflector (depth .4 km).

The models that created the corrections applied to Figures 3.27a and 3.27b are significantly different. Figure 3.28 make this comparison between these two models: Figure 3.28a is the sum of the models derived in the first and second iterations; Figure 3.28b is the model derived in one, less strongly damped iteration. Figure 3.29 shows contour plots of the same two models; it shows the details of the models. The model derived in two iterations is obviously the smoother of the two models. Furthermore, this model shows the anomaly immediately above the shallowest reflector to be narrower than does the model derived in one iteration. Note that simple smoothing of Figure 3.29a would not remove this long-wavelength feature. Recall that the broadening of the anomaly immediately above the shallowest reflector was described as a backprojection artifact. Thus, the model derived in two iterations is smoother and contains more reliable information.

The comparison in Figures 3.28 and 3.29 has illustrated the limitations of the linearization between interval slowness and stacking slowness. The iterative application of the linear theory allows the algorithm to properly account for large stacking slowness variations that cannot be entirely accounted for with a single linear function of interval slowness. Because this iterative approach requires that traveltime corrections be applied, then semblances recomputed, each iteration considerably increases the computation. Nonetheless, as shown by this example, a single additional iteration might be all that is required to explain strong lateral variations in velocity.

3.8 CONCLUSIONS

This chapter has extended the one-dimensional velocity-analysis algorithm of the previous chapter to two dimensions. Applied to data with flat reflectors, this two-dimensional algorithm can work in a fully automatic mode. Furthermore, for data with large lateral variations in slowness, an iterative application of the algorithm is appropriate. When this algorithm is applied to a field dataset with large lateral variation, the results show that laterally variable interval slownesses can be determined from stacking slownesses. Indeed the interval slownesses derived in this manner are able to explain the lateral variation in both stacking slowness and traveltime.

The strength of this velocity-analysis algorithm is that it is based on stacking slowness—a measurement that is routinely and reliably made. Furthermore, it requires no picking, and thus avoids the problems with efforts to fit poor picks. The weakness of the algorithm is that some information is lost in the transformation from traveltimes to stacking slowness. Thus, the algorithm will not be able to resolve fine details of the interval-slowness model. Nonetheless, the results show that the model constructed from

stacking slownesses can explain the main features of the laterally varying traveltimes.

The version of the algorithm presented in this chapter required flat reflectors. Chapter 4 derives a version that is valid for dipping reflectors. An alternative to the use of dipping reflectors is to remove them from the data. Thus, if the application of the velocity analysis algorithm is preceded by a dip filter on the data, the version of the algorithm presented here can be used directly. The exclusion of the dipping reflectors would only degrade the resolution of the model; the resulting model would then contain the velocity information provided by the flat reflectors.